doi.org/10.1002/celc.202000164

Solid-State Electrolyte Materials for Sodium Batteries: Towards Practical Applications

Qianli Ma*[a] and Frank Tietz[a, b]

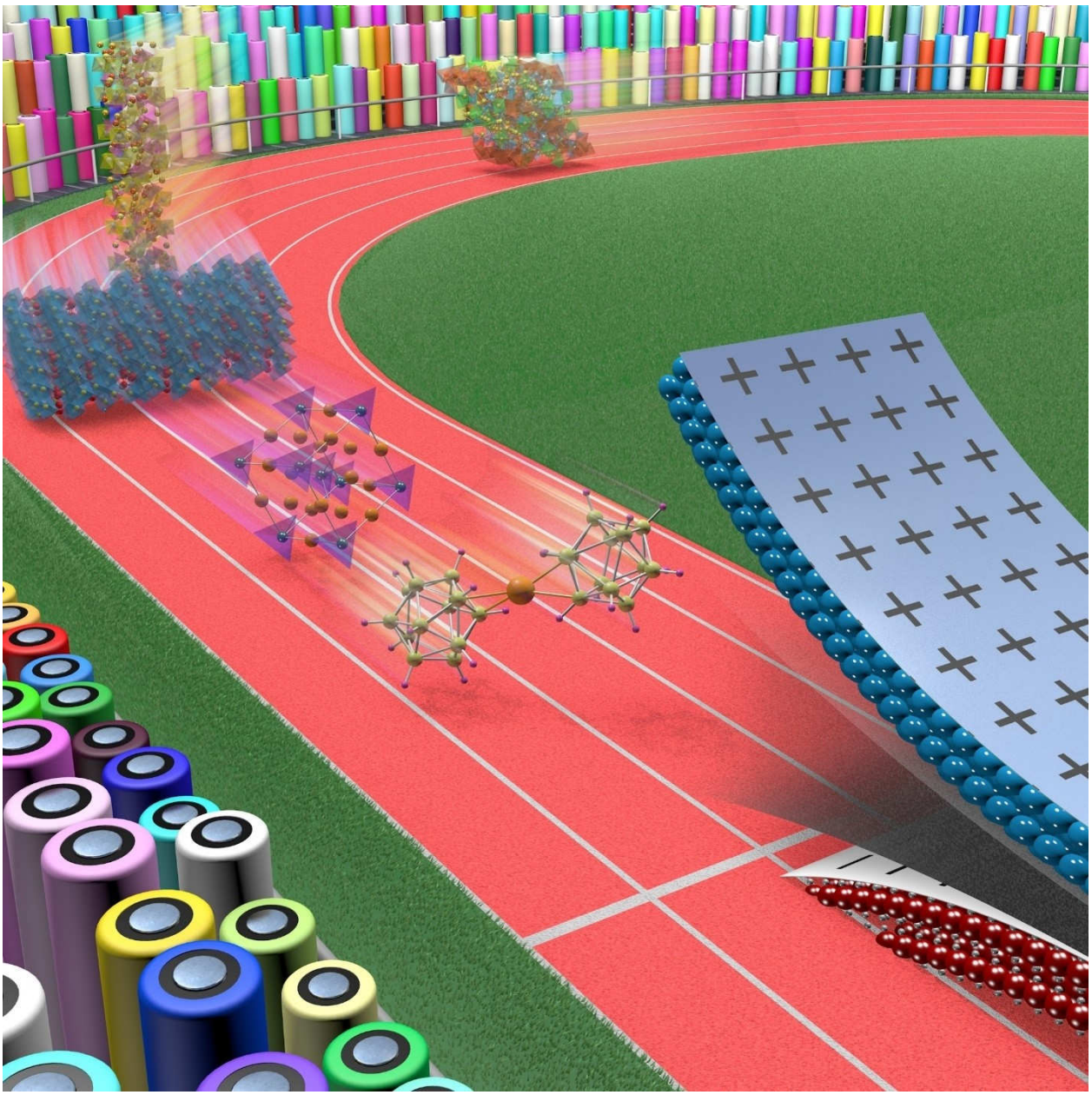

The huge demand for delocalized energy storage due to the application of fluctuating energy sources leads to a need for low-cost devices available on a large scale and with high energy density. Solid-state sodium batteries (SSNBs) show great potential in this field and have recently attracted extensive interest. Several review-type publications have already discussed fundamental materials properties and more academic aspects related to ionic transport and charge transfer. In contrast, the current Review uses state-of-the-art 18650 Li-ion batteries as a benchmark and evaluates solid-state electrolytes (SSEs) and corresponding SSNBs in terms of their practical applicability and development status. This Review summarizes recent progress based on key properties of various SSEs, such as ionic conductivities, chemical stabilities, mechanical properties, interface compatibilities with sodium metal, and compares the published SSNBs in detail with respect to galvanostatic cycling and full cell performance. It provides insights and perspectives with respect to SSEs for SSNBs and indicates the direction of future developments for the practical application of SSNBs.

1. Introduction

The combination of fluctuating energy sources, e.g. solar and wind power, and stationary energy storage systems is regarded as the most promising substitute for state-of-the-art fossil energy with respect to sustainable energy supply.[1–3] The huge demands of delocalized energy storage units of at least the MW level limit the application of state-of-the-art energy storage devices, i.e. lithium-based batteries, because of the limited abundance and increasing cost of lithium resources, while the electrochemically similar but less mature sodium-based batteries fit the requirements perfectly since stationary energy storage does not require the system to have high energy density. While the volume and weight of the devices is less important, the main focus for sodium-based batteries is directed towards low energy cost and large-scale applications including high intrinsic safety.[2–8] Parallel to their lithium counterparts, sodium-based batteries with solid-state electrolytes (SSEs) rather than liquid based electrolytes (LBEs, defined as electrolytes with liquid as the only or major conducting phase, for example liquid electrolytes, ionic liquids, gel-polymers etc.) display the advantages of non-leakage, non-volatilization, separator-free design, adaptability to temperature changes as well as compatible theoretical energy and power densities (Figure 1), and are regarded as the batteries of the next generation.[9–15] In fact, the flammability of the sodium-metal anode in water-containing environments is still questionable. However, its targeted stationary applications make the risk controllable compared to that of mobile applications. The situation can be compared with storage tanks of oil containing thousands of tons of capacity and potentially have high risk of explosion, but people will not abandon their installations because such risk is highly controllable compared to a running car. Moreover, since sodium metal has the highest specific capacity of 1166 mAh g^{-1} (in the charged state) and the lowest potential of all sodium-based anodes of −2.71 V in comparison to standard hydrogen electrodes, it complies the commercial requirement of high energy density. The very low Na content per battery cell is expected to cause a reduced thermal event and not a heavy explosion. Especially when SSEs are applied instead of LBEs, the hazard is further decreased.[16] The integrated consideration of the above arguments explains the current great interest in solid-state sodium batteries (SSNBs).[7,8,10,16–20]

Na-based SSEs have a long history of more than fifty years.[25–27] Successful examples such as sodium-sulfur and sodium-nickel chloride batteries have already been commercialized for stationary energy storage.[28,29] However, formerly (1960s to 2000s) such batteries usually had operating temperatures above the melting point of sodium metal, i.e. these batteries had at least a liquid anode and needed temperature control and complex protection systems because of the presence of liquid sodium,[26,30] as well as extra heat to maintain the operating temperature, which resulted in additional cost and reduced efficiency. In comparison, the SSNBs discussed in

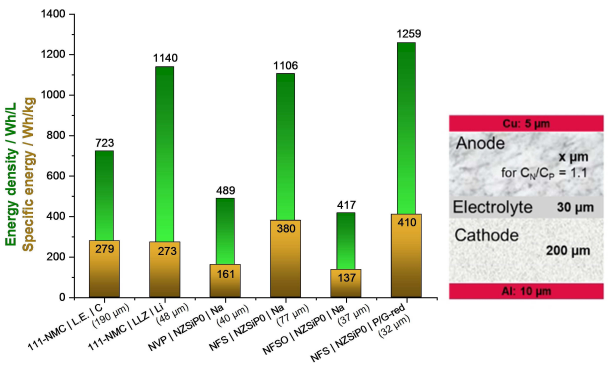

Figure 1. Comparison of the energy density (Wh l^{-1}) and specific energy (or gravimetric energy density, Wh kg^{-1}) of an LIB, an SSLB and different SSNBs on the basis of the cell architecture shown on the right-hand side. The LIB is composed of a graphite anode with 30 vol.% porosity, a $LiNi_{0.33}Mn_{0.33}Co_{0.33}O_2$ cathode with 30 vol.% porosity and a separator with 40 vol.% porosity, all filled with liquid electrolyte (1 M $LiPF_6$ in ethylene carbonate and dimethyl carbonate). In the other cases, a pure metal layer or a composite of P/C nanosheets with 40 vol% SSE is used for the calculations. The thickness of the anode is determined by a capacity excess of the anode of 10% (C_N/C_P = 1.1). The cathodes are based on composites with 60 vol.% active material and 40 vol.% SSE. Abbreviations denote 111-NMC = $LiNi_{0.33}Mn_{0.33}Co_{0.33}O_2$, L.E. = liquid electrolyte (see above), C = graphite, LLZ = $Li_7La_3Zr_2O_{12}$, NVP = $Na_3V_2P_3O_{12}$,[21] NZSiP0 = $Na_3Zr_2Si_2PO_{12}$, NFS = Na_2FeSiO_4,[22] NFSO = $Na_2Fe(SO_4)_2$,[23] P/G-red = red phosphorus-graphene nanosheet.[24]

[a] Dr. Q. Ma, Dr. F. Tietz
Forschungszentrum Jülich GmbH, Institute of Energy and Climate Research
Materials Synthesis and Processing (IEK-1), 52425 Jülich, Germany
E-mail: q.ma@fz-juelich.de
[b] Dr. F. Tietz
Forschungszentrum Jülich GmbH, Institute of Energy and Climate Research
Helmholtz-Institute Münster (IEK-12), 52425 Jülich, Germany

the past ten years mainly target applications at room temperature (RT), which avoids the disadvantages of high-temperature sodium batteries mentioned above and commercial state-of-the-art lithium-based batteries can be set as the benchmark (see Figure 1).

Because of their prospective potential, SSNBs have received considerable attention in recent years and some review publications can already be found,[16–20,31] and fundamentals of the field have been both intensively and extensively overviewed in detail. Nevertheless, the ultimate target of this research is practical application of the system. In the current review, the comprehensive collection of data on solid electrolytes will not only give an update on the available materials,[20,32] but also an evaluation of practical applicability in SSNBs by summarizing recent progress. The key parameters of SSEs, such as ionic conductivities, chemical stabilities, interface compatibilities with sodium metal, galvanostatic cycling performances and mechanical properties, are discussed in detail. The key challenges and an outlook for SSNB development are also given.

For historical reasons, inorganic SSEs are often mentioned first in the context of sodium batteries, but there are also many new developments in the field of polymer electrolytes. During the past decade enormous progress has been made with various types of organic electrolytes and recent review papers are available for most of them, e.g. for ion-gels,[33] ionic polymers, and plastic crystals based on ionic liquids,[34] diversification of conventional polymers by copolymerization and multiple combinations to form composite and hierarchical electrolytes.[35] In view of the above-mentioned up-to-date reviews, we will concentrate in the following on the inorganic solid electrolytes, and will also try to define "solid-state polymers", separate them from other polymer electrolytes, and discuss them in comparison to inorganic solid electrolytes.

2. Discussion on Key Parameters of SSNBs

To date, no RT-SSNBs have yet been successfully commercialized. For the discussion of SSNBs towards their practical applications in future, it is necessary to briefly describe the existing types of rechargeable batteries in the market. Today there are three main types of rechargeable batteries available now, namely lead-acid battery, nickel-metal hydride battery and Li-ion battery (LIB). Among these types, the lead-acid battery is the most cost-effective type, but it also has the lowest gravimetric energy density (35–40 Wh kg^{-1}). Moreover, the lead-acid battery also causes environmental impacts because of the toxic lead compounds, even though the recycling of these batteries is very much established. Lead-acid batteries are popular as auxiliary power source for cars, as well as for stationary applications like grid energy storage. The nickel-metal hydride battery shows higher gravimetric energy density than the lead-acid battery (60–120 Wh kg^{-1}) and is mainly applied in digital devices. Compared to the other two types, the nickel-metal hydride battery has an unpleasant memory effect during charge and discharge. Comparatively, LIB is the most popular available secondary battery type nowadays because it shows the highest gravimetric energy density (100–300 Wh kg^{-1}), as well as long cycle life, high charge/discharge rates etc.[1–3,15] LIB is extensively applied in both mobile and stationary devices because of its excellent electrochemical properties. The battery size 18650 (18 mm in diameter, 65 mm long) is one of the most representative designs for LIBs. It has received special notice because the well-known electric car producer Tesla applies these batteries as the basic power unit in their cars. Therefore, in the present study significant parameters of the LIB, in particular the commercial 18650 battery size, is used as the most meaningful benchmark as listed in Table 1.[36,37] For the future commercialization of SSNBs, the discrepancy should not be high, although it is not necessary for all the criteria in Table 1 to be satisfied because stationary applications are targeted and not mobile devices. On the one hand, the properties of an electrolyte material in SSNBs, i.e. the conductivity and interface resistance with electrodes, strongly influence the internal resistance, chemical stability and interface compatibility with the electrode, and, on the other hand, they are also decisive for longevity. The design of the cell architecture has an impact on both the above-mentioned factors and the energy density of the full cell. The mechanical properties are also important in practical applications of the batteries in terms of manufacturing reliability and definition of maximum dimensions of the batteries. There are already several

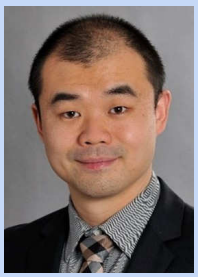

Qianli Ma obtained his B.S. and Ph.D. degrees at the University of Science and Technology of China, majoring in materials science. From 2007 to present, he has been working in the Forschungszentrum Jülich, IEK-1 (Germany), first as post-doc, then as senior scientist, and now as tenure scientist. He specializes in the development of non-metallic inorganic materials. He has detailed research experience with the relationships between processing, microstructure and properties, and is especially familiar with the research and development of solid-state batteries and fuel cells.

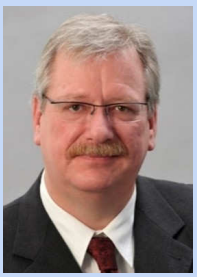

Frank Tietz received his Ph.D. degree in solid-state chemistry from the University of Hanover (Germany). After a Humboldt fellowship at the University of Trento (Italy), he joined Forschungszentrum Jülich (Germany) in 1995. He has worked on a wide variety of ceramic materials at both fundamental and technology development level, including superconductors, cationic and anionic conductors, mixed ionic-electronic conductors as well as ceramic/metal composite materials. Initially working on high-temperature materials for solid oxide fuel cell development and thermal barrier coatings, his current work focuses on new electro-ceramic materials for different types of solid-state batteries.

Table 1. Some key parameters of the commercial 18650 batteries.

Working voltage [V]	Working C-rate	Capacity [mAh]	Internal resistance [mΩ]	Electrode area [cm^2]	Longevity (cycle count)	Mass [g]	Volume [cm^3]
2.4–4.2	0.2–1.0	1500–3500	10–40	400–600	> 1000	40–50	16.5

candidate systems as electrolyte materials for SSNBs, which will be discussed in the following sections with respect to the above key parameters.

2.1. Conductivities

The resistance of the electrolyte material itself contributes directly to the internal resistance of the battery cell. Hence, high conductivity is a necessity for the candidate material. The area-specific resistance (ASR) of a separator in current commercial LIBs can be considered as a rough estimate. The ASR of a single component can be written as Equation (1):

$$\mathrm{ASR} = L/\sigma \quad (1)$$

where L indicates the thickness and σ indicates the conductivity of the component. For example, a 25 μm thick film of pure liquid electrolyte with $\sigma = 1 \times 10^{-2}\ \mathrm{S\,cm^{-1}}$ results in an ASR value of 0.25 $\Omega\,cm^2$.[38,39] However, the application of a porous separator in LIBs increases this value to 3.75 $\Omega\,cm^2$ due to the tortuosity of the membrane.[40],[41] Since the cationic conductivity is only a fraction of the total conductivity in the liquid electrolytes, an even higher area-specific resistance can be assumed. In order to achieve the above-mentioned ASR value with a 10 or, more realistically, a 30 μm thick SSE, this membrane should have an ionic conductivity of 2.7 or $8.0 \times 10^{-4}\ \mathrm{S\,cm^{-1}}$, respectively. Similar conductivity values are obtained when the total ASRs of LIBs, varying between 4 and 24 $\Omega\,cm^2$, is considered (Table 1) and when the values are fully determined by the electrolyte material. Then the conductivity of the SSE material should correspond to 2.5 and $0.4 \times 10^{-4}\ \mathrm{S\,cm^{-1}}$, respectively, in the case of a thin electrolyte layer of 10 μm. This estimation, imprecise though it is, fits well with the general opinion that the total ionic conductivity (σ_{total}) of the solid-state electrolyte should be at least $> 10^{-4}\ \mathrm{S\,cm^{-1}}$, and it would be better for it to be higher than $10^{-3}\ \mathrm{S\,cm^{-1}}$ at RT.[42,43] At the same time, to avoid self-discharge, the electronic conductivity (σ_e) of the material should be at least lower than $10^{-8}\ \mathrm{S\,cm^{-1}}$.[43]

Another benchmark can be derived from Na/S and Na/$NiCl_2$ batteries and the ionic conductivity of the solid electrolytes at high temperature. Figure 2a shows the temperature dependence of the ASR for two ß/ß" alumina from the literature and from a commercial manufacturer for different component thicknesses.[44–46] The temperature dependence of the cell-ASR of a Na/$NiCl_2$ battery and its electrolyte-ASR is also shown.[47] When the thickness of the electrolyte components is 1.5 mm, the ASR increases steadily from 0.7 $\Omega\,cm^2$ at 300 °C to about 133 $\Omega\,cm^2$ at 25 °C. This means that the electrolyte may only be

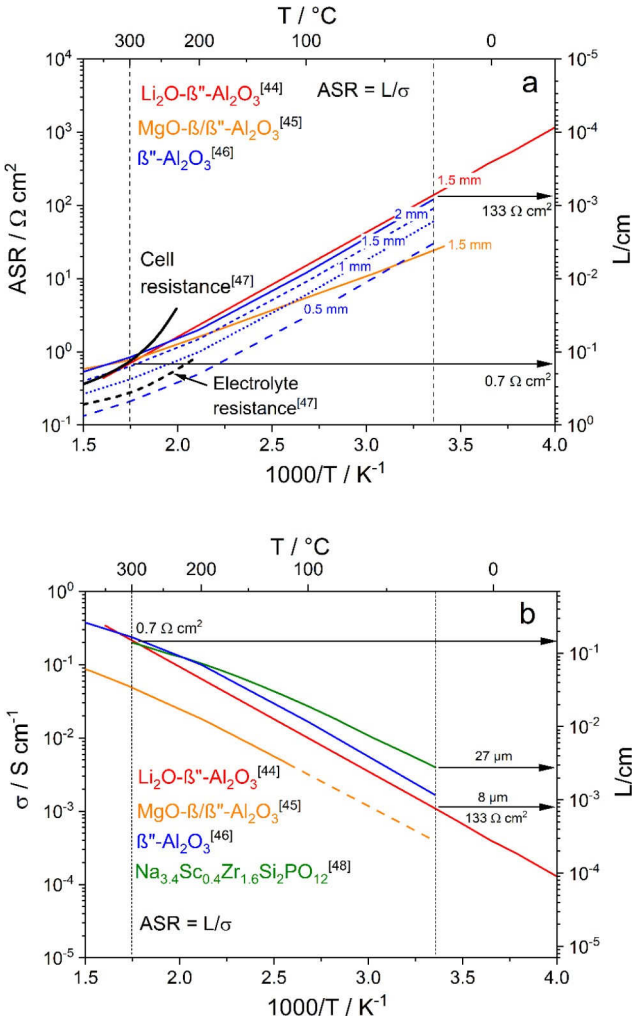

Figure 2. a) Temperature dependence of the ASR for different ß/ß"-aluminas and a Na/$NiCl_2$ battery and its electrolyte (black curves). b) Comparison of the conductivity of different ß/ß"-aluminas together with a very well conducting NaSICON material ($Na_{3.4}Sc_{0.4}Zr_{1.6}Si_2PO_{12}$). For the same ASR values, the corresponding layer thicknesses can be read on the right-hand scale.

8 μm thick to obtain the same ASR as at 300 °C. This approach can be transferred to Figure 2b, where the conductivity of the electrolytes is shown. With the ASR values determined from Figure 2a, the conductivities can be scaled with the thickness of the components. Apparently, a more conductive electrolyte allows larger thicknesses. As an example, a material with a conductivity of $4 \times 10^{-3}\ \mathrm{S\,cm^{-1}}$ at 25 °C, $Na_{3.4}Sc_{0.4}Zr_{1.6}Si_2PO_{12}$ (NSZSP0.4),[48] may then allow an electrolyte thickness of 27 μm instead of 8 μm to achieve the same ohmic resistance – a thickness that can realistically be achieved with ceramic manufacturing methods and can be defined as the target thickness for Na batteries at RT (see also Figure 1). In principle,

SSE materials with even higher conductivity will greatly simplify component preparation.

In the following sections, the ionic conductivity of various Na^+ ion conductors is presented. For better comparison, the Arrhenius diagrams have constant axis intercepts. In studies in which a series of compositions or preparation methods have been investigated, only the material with the highest conductivity is shown. In all the figures, the values of σ_{total} are shown because these data are more relevant for technical applications than bulk conductivity (σ_b), even though the σ_{total} values result in a larger scatter of the data due to the varying contributions of the grain boundary conductivities and porosity of the materials.

2.1.1. NaSICONs

In 1976, Hong et al. discovered $Na_{1+x}Zr_2(SiO_4)_x(PO_4)_{3-x}$ (NZSP), which has high Na-ion conductivity of 0.2 $S\,cm^{-1}$ at 300 °C.[49,50] In the following years, it was observed that the composition of the material has very high flexibility with respect to substitutions without changing the crystal structure apart from distortions. Up to now, hundreds of compositions have been reported originating from NZSP.[51] Because of their identical origin, similar structure and high conductivity, these materials are summarized under the name of NaSICON, which is the abbreviation for Na superionic conductors.

Before discussing the conductivity of the NaSICONs, the large scatter of the compiled conductivity data should be clarified. Figure 3 shows the Arrhenius plot of the very first and extensively studied NaSICON, $Na_3Zr_2Si_2PO_{12}$, reported in various references. Although nominally exactly the same composition, different references gave deviations of up to one order of magnitude for σ_{total}, i.e. from 1×10^{-4} to 1×10^{-3} $S\,cm^{-1}$ at 25 °C. Two facts can be obtained from Figure 3. Firstly, the development of the NaSICON is mature. There are plenty of data

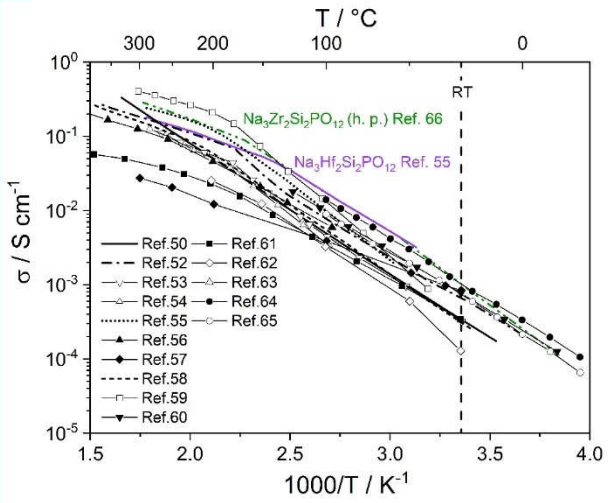

Figure 3. Temperature dependence of the σ_{total} of $Na_3Zr_2Si_2PO_{12}$ reported in different references.[50,52–65] For comparison a hot-pressed sample (h. p.)[66] and a hafnium analogue are shown.[55]

sources and several of them confirm a maximum conductivity of 1×10^{-3} $S\,cm^{-1}$. Secondly, since the deviation of the data is high, a correct understanding of the conductivities of NaSICONs is difficult due to a frequent lack of further information on the investigated samples. In recent years, the explanation of the published scatter of σ_{total} has become clear. Theoretically, a polycrystalline material with fixed composition, fixed sintering conditions and at a fixed testing temperature should show the same bulk conductivity (i.e. conductivity within a single grain, σ_b). However, σ_{total} consists of both σ_b and grain-boundary conductivity (contributed by the grain boundaries and other microstructural imperfections of the polycrystalline material, σ_{gb}). It is known that during sintering of NaSICON materials, the lattice parameters *a* and *c* of the rhombohedral phase change differently (monoclinic NaSICONs undergo a phase transition to the rhombohedral phase above 200 °C), i.e. the thermal expansion coefficient (TEC) of lattice parameters *a* and *c* is very different. Such thermal expansion anisotropy (TEA) causes contact losses or microcracks along the grain boundaries.[48,67] Therefore the σ_{total} of NaSICONs can be greatly decreased by the sintering conditions and abnormal decrease of σ_{gb}. Little attention was previously paid to the separation of σ_b from σ_{total}. On the one hand, because targeted conductivities at 300 °C do not require and cannot deliver this information, and, on the other hand, due to the lack of necessary experimental equipment. However, recently several reports gave a clear differentiation of σ_b from σ_{total} for $Na_3Zr_2Si_2PO_{12}$, and are in close agreement of 2×10^{-3} $S\,cm^{-1}$ at 25 °C.[48,64,65,67] This indicates that the σ_{total} may be one to two orders of magnitude lower than the σ_b because of the dominant contribution of σ_{gb}. Since σ_{gb} is significantly influenced by sample preparation processes resulting in different microstructures (grain sizes, density, microcracks, impurities, etc.),[68] it is not surprising that the different references in Figure 3 show a large scatter of σ_{total}.

NaSICONs have the generic formula of $AM_2X_3O_{12}$. Compounds with this formula were first investigated in the 1880s,[69] then again in the 1960s,[70] and a mineralogical example was described as recently as 1993.[71] A represents alkali ions, M stands for tetravalent cations and X is usually phosphorus. When M is replaced by trivalent ions (M′), this leads to the formula $A_3M'_2X_3O_{12}$, whereas the replacement of X by tetravalent ions ($X' = Si^{4+}$, Ge^{4+}) leads to the end member $A_4M_2X'_3O_{12}$ with full occupation of the available A-sites. A further increase of the A content is only possible with partial substitution and occupancy on the M-sites, e.g. $Na_5ZrP_3O_{12}$ (i.e. $Na_4(NaZr)P_3O_{12}$).

Figure 4 shows the high σ_{total} of different kinds of NaSICONs.[48,64,67,72–77] As a reference, the σ_{total} of original $Na_3Zr_2Si_2PO_{12}$ can now reach 1×10^{-3} $S\,cm^{-1}$.[64] Until now, the NaSICONs with the highest σ_{total} are all variations of this composition. The substitution of lower-valent ions on the Zr position is compensated by a higher content of Na in the formula and can normally increase the conductivity of the system.[48,72,73,76,77] The same effect can also be achieved by changing the ratio of Si and P and increasing the Na content accordingly.[67] The same rules are also valid for other NaSICON systems, e.g. using Hf or Sc as the transition metal in the formula.[74,75] Interestingly, in the generic formula of A_{1+x+}

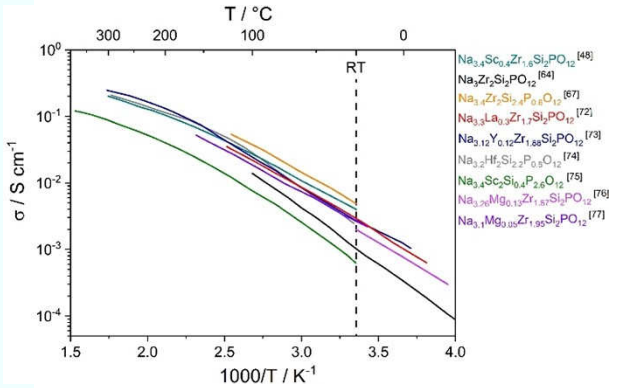

Figure 4. Temperature dependence of the σ_{total} of NaSICON materials with different Zr substitutions and Na contents.

$_yM'_xM_{2-x}Si_yP_{3-y}O_{12}$, there seems to be an optimum Na content of about 3.4 mol per formula unit (f. u.). In several publications it has been proven that the σ_{total} of the optimum formula is higher than for other compositions in the same system with higher or lower Na content.[48,67,72,75] Ma et al. attributed this phenomena to the accomplishment of the best ratio between occupied and vacant Na sites in the NaSICON unit cell, where the requirements of high conductivity, i.e. high concentration of charge carriers and significant number of Na vacancies, are both satisfied in order to permit fast Na ion transport.[48,67] The point is also supported by some modelling investigations.[65,78]

All the compositions in Figure 4 satisfy the minimum requirement of SSEs with respect to σ_{total} ($>10^{-4}$ S cm^{-1} at RT). The sample with the lowest σ_{total} in Figure 4, $Na_{3.4}Sc_2Si_{0.4}P_{2.6}O_{12}$, still has a value of 7×10^{-4} S cm^{-1} at RT.[75] All other samples in Figure 4 satisfy the above defined requirement of SSEs to σ_{total} ($>10^{-3}$ S cm^{-1} at RT). The sample with the highest σ_{total} in Figure 4, $Na_{3.4}Zr_2Si_{2.4}P_{0.6}O_{12}$ has a value of 5×10^{-3} S cm^{-1} at 25 °C,[67] which is also on the same level as the state-of-the-art liquid-based electrolytes for sodium-ion batteries,[39,79] indicating the high potential of NaSICONs in solid-state batteries and other electrochemical devices.

The electronic conductivity (σ_e) is generally regarded as negligible in NaSICONs.[32,77] In specific, Song et al. confirmed that $Na_{3.1}Zr_{1.95}Mg_{0.05}Si_2PO_{12}$ shows σ_e of only 1.3×10^{-8} S cm^{-1} at room temperature.[77]

2.1.2. Beta-Alumina

β-alumina was first named by Rankin and Merwin in 1916 after investigation of the phase diagram of the CaO-MgO-Al_2O_3 system and identification of a special crystal structure,[80] which at that time was regarded as an isomorph of Al_2O_3. Ridgway et al. first reported the presence of Na_2O in this compound, which has the empirical formula $Na_2O\cdot11\ Al_2O_3$ in 1936,[81] which has the empirical formula $Na_2O\cdot11\ Al_2O_3$. Later in 1962, Thèry et al further studied the Na_2O–Al_2O_3 system and found another compound with the empirical formula $Na_2O\cdot5\ Al_2O_3$,[82] known as β″-alumina. Finally, in 1968, Yamaguchi et al. reported the last member of the family, β′-alumina,[83] which has the formula $Na_2O\cdot7\ Al_2O_3$. The compounds in the β/β′/β″-alumina family all display great similarity in their crystal structure. Especially for β- and β′-alumina, their similarity is so great that they were customarily uniformly categorized as β-alumina.[84] In both β- and β″-alumina, the Na^+ ions can be substituted by other elements such as K, Ag, Ca, Mg and even trivalent cations without changing the crystal structure.

β-alumina crystallizes with a hexagonal structure (space group of $P6_3/mmc$),[83] while β″-alumina displays a rhombohedral structure with the space group $R\bar{3}m$.[85] The diffusion of the sodium ions in β/β″-alumina occurs two-dimensionally in conduction planes perpendicular to the *c*-axis. The motion of the sodium ions parallel to the *c*-axis is blocked by closely packed spinel layers,[84] i.e. β/β″-alumina is a highly anisotropic ion conductor with excellent Na^+ ion conduction in the planes perpendicular to the *c*-axis, while it is an insulator in the direction of the *c*-axis. Consequently, although the conductivity of single-crystalline β/β″-alumina can be as high as >0.1 S cm^{-1} (at RT) along the conduction planes,[86,87] the total conductivity of polycrystalline β/β″-alumina is much smaller (Figure 5) because in freely arranged polycrystalline grains the sodium ion conduction path may be blocked by the mixed orientation of the grains. Since the cost of single-crystalline β/β″-alumina is not acceptable in practical applications, this section focuses on the conductivity of polycrystalline β/β″-alumina. Figure 5 shows the Arrhenius plots of representative polycrystalline β/β″-aluminas.[44,45,60,84,88–91] Scattered conductivity values are also observed here, ranging from 3×10^{-4} S cm^{-1} to 5×10^{-3} S cm^{-1}. As mentioned above, this is mainly due to the disorientation of the grains in the polycrystalline structure. In most cases, the processing of the materials results in microstructures in which the grains show random orientation leading to a conductivity of about 1×10^{-3} S cm^{-1}. One exception in Figure 5 is the investigation by May et al.,[45] where they applied a seeding technique to control the lattice direction of the grains in the polycrystalline structure and achieved a high conductivity of 6×10^{-3} S cm^{-1}. Also, the use of nanopowders in combination with

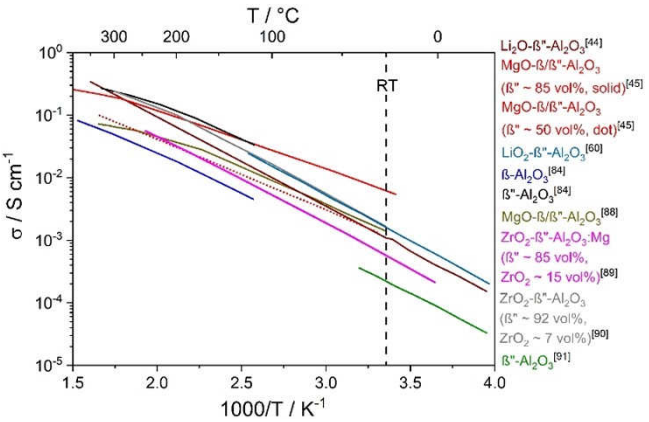

Figure 5. Temperature dependence of the σ_{total} of different polycrystalline β/β″-aluminas stabilized with different elements.

sintering aids (TiO_2, ZrO_2) led to very dense and highly conductive β/β″-aluminas of up to 5.4×10^{-3} S cm^{-1}.[92]

β/β″-aluminas also show negligible σ_e of 10^{-10}–10^{-11} S cm^{-1} at room temperature.[87,93]

2.1.3. Other Oxides and Oxide Glasses

Because of the benefits of high stability and low cost compared to other sodium ion conductors, oxides or oxide glasses are specifically addressed in this section. Figure 6 shows the Arrhenius plots of miscellaneous oxides and oxide glasses other than NaSICONs and β/β″-aluminas, including $Na_5LnSi_4O_{12}$ ceramics or partially crystallized glass-ceramics (Ln = La-Lu and Y),[94–98] Na_2O–P_2O_5–SiO_2 based glass-ceramics,[99–101] $Na_2X_2TeO_6$ ceramic series (X = transition metal)[102,103], Na_2O–TiO_2 based ceramics,[104] and glasses of various compositions.[97,105,106] In general, crystalline ceramics (or glass-ceramics) show higher conductivity compared to pure glasses (Figure 6), because regularly arranged atoms in crystalline ceramics have a long-range order and can form conduction paths for Na ions, while single ionic jump mechanisms dominate sodium diffusion in materials with short-range order, such as glasses, where higher activation energy is needed.[105]

As the most conductive materials in Figure 6, the $Na_5LnSi_4O_{12}$ series was first reported by Maksimov et al. in 1969.[107] The silicates show a rhombohedral phase in a space group of $R\bar{3}c$ or $R\bar{3}$.[108] However, the preparation of single-phase $Na_5LnSi_4O_{12}$ is rather difficult, because a small number of secondary phases, especially glassy phases, are always found in the final product.[94,95,97,101] Although in general glasses display lower conductivity compared to ceramics, proper amounts of glassy additives may induce densification and improvements in ionic conductivity at grain boundaries of a polycrystalline ionic conductor,[97] which is also the principle of glass-ceramics. Sadaoka et al. deliberately added a Na_2O–Y_2O_3–SiO_2 glassy phase into $Na_5YSi_4O_{12}$ to increase the density and conductivity of the final product.[97] Beyeler et al. measured the single-crystal conductivity (i.e. σ_b) of $Na_5YSi_4O_{12}$ and obtained 3.2×10^{-3} S cm^{-1} and 8.0×10^{-3} S cm^{-1} (RT) parallel and perpendicular to the *c*-axis,[108] respectively, while the corresponding σ_{total} of $Na_5YSi_4O_{12}$ and other $Na_5LnSi_4O_{12}$-based materials is typically about 1×10^{-3} S cm^{-1} at RT (Figure 6). Such high conductivity determines the great potential of $Na_5LnSi_4O_{12}$-based materials such as SSEs for SSNBs, but these materials have not been extensively studied as yet. With respect to the NaSICON materials, substitutions may further improve the conductivity of the $Na_5YSi_4O_{12}$ system. Although other Na_2O–Ln_2O_3–P_2O_5–SiO_2-based glass-ceramics have also been investigated,[99–101] their conductivity is not only much lower than the $Na_5LnSi_4O_{12}$ series, but also lower than the minimum requirement of SSEs with respect to σ_{total} (10^{-4} S cm^{-1} at RT). $Na_5LnSi_4O_{12}$ also shows very low σ_e.[95,98,108] The value is only ~10^{-12} S cm^{-1} at room temperature.[108]

Other oxide ceramics or glass ceramics have been even less thoroughly investigated compared to the $Na_5LnSi_4O_{12}$ system. $Na_2X_2TeO_6$ ceramics, which crystallize in a hexagonal structure (space group $P6_322$), were first reported as SSEs by Evstigneeva et al. in 2011,[102] . Additionally, Na_2O–TiO_2-based ceramics also have a hexagonal structure,[104] but have not yet attracted much interest, although the Li_2O–TiO_2 analogues have been intensively studied as ion conductors with perovskite structure.[109] As yet, these two series show conductivities just above the minimum requirement of SSEs. However, since only a very limited number of studies have been published so far, there is still potential in the two series for improving the conductivity. Some pure glasses of Na_2O–Na_2S–P_2O_5,[106] Na_2O–Y_2O_3–SiO_2[97] and Na_2O–B_2O_3–SiO_2[105] are also included in Figure 6. However, their conductivity is in the range of 10^{-6} S cm^{-1} or less at RT, which is not really favorable for SSEs. As mentioned above, the lack of long-range order makes ionic conduction more difficult in glasses than in crystals.

2.1.4. Sulfides and Chalcogenides

Figure 7 shows the Arrhenius plots of σ_{total} of Na-ion conducting sulfide or chalcogenide ceramics, glass-ceramics or glasses.[10,110–123] Recent attention to sulfide (or chalcogenide) ceramics or glass-ceramics started from Na_3PS_4 reported by

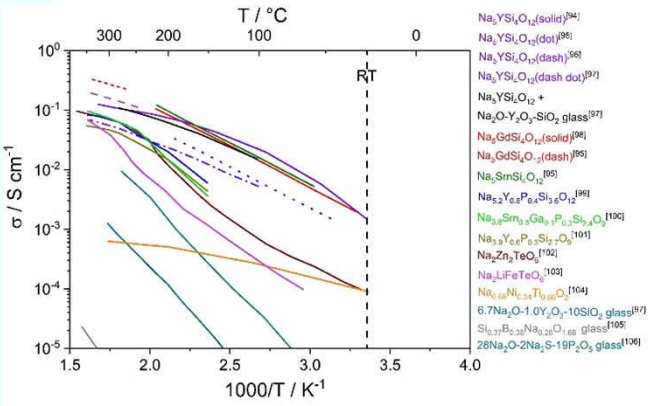

Figure 6. Temperature dependence of the σ_{total} of miscellaneous Na-ion conducting oxides (oxide glasses) other than NaSICONs and β/β″-aluminas. Compositions of glasses are given in molar ratios.

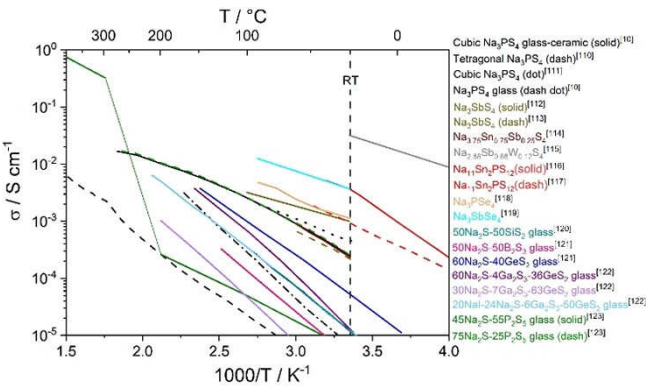

Figure 7. Temperature dependence of σ_{total} of sulfide (or chalcogenide)-ceramics, glass-ceramics or glasses.

Hayashi et al. in 2012,[10] which has been influenced by the increasing significance of lithium-sulfides as lithium fast ionic conductors.[124] Although Na_3PS_4 had long been reported,[110] Hayashi et al. were the first to report the cubic phase of Na_3PS_4 rather than the formerly known tetragonal phase. The phase change leads to a leap in conductivity from 1×10^{-6} S cm^{-1} to 2×10^{-4} S cm^{-1} at RT,[10] which was further increased to 5×10^{-4} S cm^{-1}.[111] Some materials with similar compositions, e.g. Na_3SbS_4 and $Na_{3.75}Sn_{0.75}Sb_{0.25}S_4$,[112–114] were subsequently reported. Although the materials have a tetragonal crystal structure, their conductivities are similar to that of Na_3PS_4, and also reach $\sim2\times10^{-4}$ S cm^{-1} at RT. A breakthrough was achieved very recently when Hayashi et al. reported a superior conductivity of 3.2×10^{-2} S cm^{-1} at RT for $Na_{2.88}Sb_{0.88}W_{0.12}S_4$,[115] which also displays a cubic structure. The conductivity is even higher than the best lithium thiophosphate: $Li_{9.54}Si_{1.74}P_{1.44}S_{11.7}Cl_{0.3}$ (2.4×10^{-2} S cm^{-1}),[13] which exhibits the highest conductivity of all the reported lithium ion conductors. A small technical trick was used for $Na_{2.88}Sb_{0.88}W_{0.12}S_4$ to achieve this superior conductivity: a pressure of over 1 GPa was applied to the sample during preparation. Since sulfide ceramics have limited ductility, it is possible that the super-high pressure decreased the grain-boundary resistance of the sample to the minimum. Another series of $Na_{11}Sn_2PS_{12}$ was reported almost simultaneously by two groups,[116,117] and shows great similarity to its lithium counterpart $Li_{10}GeP_2S_{12}$.[124] Although the conductivity of $Na_{11}Sn_2PS_{12}$ (1–4×10^{-3} S cm^{-1} at RT) is significantly lower than that of $Li_{10}GeP_2S_{12}$ (1.2×10^{-2} S cm^{-1}), it is still favorable for application as an SSE. Similar to sulfide ceramics (or glass-ceramics), other chalcogenide-based materials also show their potential with respect to conductivity. Na_3PSe_4 was first reported by Zhang et al.,[118] followed by $Na_3P_{1-x}Sb_xSe_4$ reported by Wang et al.[119] Similar to Na_3PS_4, these materials show a cubic structure and exhibit even higher conductivities. Na_3PSe_4 has a conductivity of 1.2×10^{-3} S cm^{-1} at RT, while Na_3SbSe_4 displays a conductivity of 3.7×10^{-3} S cm^{-1}. Evidently, when the composition of Na_3PX_4 (X = O, S, Se) changes with X along the group VI elements, the conductivity of the composition also increases accordingly. At RT, Na_3PO_4 has a conductivity of only $\sim10^{-9}$ S cm^{-1},[125] while the conductivity of Na_3PS_4 leaps to 2×10^{-4} S cm^{-1}, and the conductivity of Na_3PSe_4 is further increased to 1.2×10^{-3} S cm^{-1}. Such a change is reasonable because the bond length in P-X and Na-X increases with the atomic number, while the bond energy decreases. In general, these steric modifications decrease the geometric difficulty and activation energy for the diffusion of Na ions and result in higher conductivity. For the same reason, Na_3SbSe_4 also exhibits higher conductivity compared to Na_3PSe_4. Based on such a principle, in general it is always easier to find a composition with higher conductivity in sulfides compared to the oxides. This has been proven with lithium conductors,[13] and is similarly correct for sodium conductors. With respect to the sulfide-glasses, similar conclusions can be drawn compared to oxide-glasses. Due to the lack of long-range order in the structure, their conductivities are significantly lower than those of ceramics or glass-ceramics. In Figure 6, none of the glasses shown passed the minimum requirement for SSEs.[120–123]

The σ_e of sulfides and chalcogenides is also low.[112,115,117,118,126] Among them, Na_3SbS_4 shows an σ_e of 1.9×10^{-10} S cm^{-1};[112] $Na_{11}Sn_2PS_{12}$ 6.0×10^{-9} S cm^{-1};[117] $Na_{2.88}Sb_{0.88}W_{0.12}S_4$ 6.0×10^{-9} S cm^{-1},[115] and Na_3PSe_4 1.4×10^{-9} S cm^{-1};[118] all values measured at room temperature.

2.1.5. Boranes

Na-ion conducting borane is a relatively new category of sodium conductor, starting from the $Na(BH_4)$–$Na(NH_2)$ system reported by Matsuo et al. in 2012,[127] which received considerable attention when monocarba-*closo*-borate salts were reported to have superior conductivity at RT by Tang et al.[128,129] Initially, sodium-*closo*-borate salts ($Na_2B_{10}H_{10}$ and $Na_2B_{12}H_{12}$) showed remarkable conductivities at their high temperature phases.[130,131] Based on this fact, similar compositions were investigated with the aim of decreasing the phase transition temperature to achieve high conductivity at RT. As a first example, $NaCB_{11}H_{12}$ was found to show a low-temperature phase in the ordered orthorhombic structure and a high-temperature phase in the disordered face-centered-cubic structure, with a transition temperature of 356 K.[132] Then $NaCB_9H_{10}$ was reported to exhibit a low-temperature phase in the ordered orthorhombic structure and a high-temperature phase in the disordered hexagonal structure and a much lower transition temperature of 323 K.[128] Moreover, Tang et al. further reported the composition of $Na_2(CB_9H_{10})(CB_{11}H_{12})$, which has a similar structure to $NaCB_9H_{10}$ with an even lower transition temperature of 310 K.[129] Figure 8 shows the Arrhenius plots of σ_{total} of Na-ion conducting boranes,[129,133] where $Na_2(CB_9H_{10})(CB_{11}H_{12})$ shows an unprecedented conductivity of 6×10^{-2} S cm^{-1} at 300 K. This value is currently the highest of all the polycrystalline sodium ion conductors. Although the transition temperatures of both $NaCB_9H_{10}$ and $Na_2(CB_9H_{10})(CB_{11}H_{12})$ are higher than RT, Tang et al. claimed that the high-temperature phases can also exist at lower temperatures because of their high stability even at lower temperatures.[128,129] $NaCB_9H_{10}$ can stably display its high temperature phase at RT with a conductivity of 3×10^{-2} S cm^{-1}. Even at 285 K, the high temper-

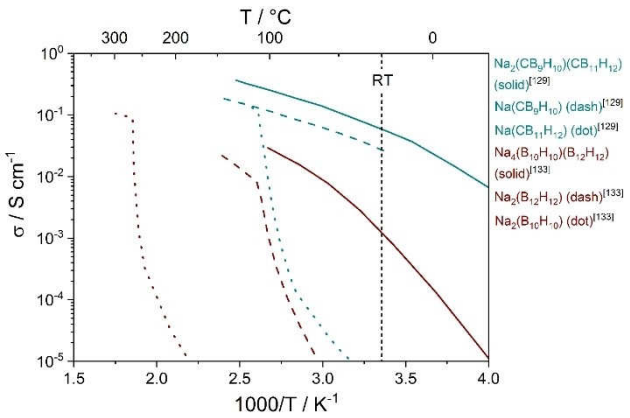

Figure 8. Temperature dependence of the σ_{total} of Na-ion conducting boranes.

ature phase can still remain. $Na_2(CB_9H_{10})(CB_{11}H_{12})$ even remains in the high-temperature phase down to 243 K and exhibits a conductivity of 5×10^{-3} S cm^{-1} at this temperature. Clearly, other sodium boranes such as $Na_2B_{10}H_{10}$, $Na_2B_{12}H_{12}$ and $NaCB_{11}H_{12}$ have no such exceptional properties. Their transition temperatures can be clearly seen by the inflection point in the Arrhenius plots (Figure 8). One exception is $Na_4(B_{10}H_{10})(B_{12}H_{12})$, which is the product of an equimolar mixture of $Na_2B_{10}H_{10}$ and $Na_2B_{12}H_{12}$. However, although it shows almost the same face-centered-cubic crystal structure as the high-temperature phase of $Na_2B_{10}H_{10}$, it has no inflection point in the Arrhenius plot like the other borohydrides from 573 K down to 233 K, which is attributed to temperature-dependent anion dynamics within the respective crystal structures.[133] Nevertheless, the conductivity of $Na_4(B_{10}H_{10})(B_{12}H_{12})$ is remarkably high with 0.9×10^{-3} S cm^{-1} at 20 °C.

The σ_e of boranes has not been explicitly determined because of its early stage of development. However, it is generally assumed that their electronic conductivity is negligible.[127,132]

2.1.6. Solid-State Polymers

As mentioned in the Introduction section, presently various types of organic electrolytes exist, such like classical polymers, co-polymers, cross-linked polymers as well as ion-gels, ionic polymers, and plastic crystals based on ionic liquids. They could all be named as "solid-state electrolyte" or "all-solid-state electrolyte" just according to their apparent appearance in their publications, ignoring whether solvent or other kind of liquid is present in the polymer structure. Here we disagree to name any liquid-containing (solvent, ionic liquid and so on) polymer as "solid-state", because apparently the mechanism of Na-ion conduction in these electrolytes is based on the liquid phase instead of the solid component. When they are compared with oxides or sulfides as so-called solid electrolytes or solid-state electrolytes, it makes the term "solid" to some extent inaccurate. Several reports with precise nomenclature categorized them as "quasi-solid-state" electrolyte, which is more appropriate. In this review, only liquid-free polymers, i.e. solid polymers composited with other solid components like salts or oxides are regarded as "solid-state polymer electrolytes".

The research on ion-conducting solid-state polymers started in the 1970's, when Fenton et al. investigated the ionic conductivity of poly(ethylene oxide) (PEO) complexes with alkali metal salts.[134] Since then, PEO has always been the main polymer phase for solid-state polymers. The reasons include:[135] Firstly, PEO has comparatively low glass-transition temperatures (−60 °C). A low glass-transition temperature is highly correlated to high polymer flexibility, while a more flexible backbone is naturally beneficial for conductivity. Secondly, although PEO has a rather low dielectric constant in comparison with many other polymers, it is a very good complexing agent for alkali metal ions, which also supports the ionic conductivity. And thirdly, the electrochemical stability of PEO is qualified for the application in Li or Na batteries. Hence, until today, more than half of the published solid-state polymers are based on PEO backbones.

In general, solid-state polymers received massive interest of research and some of them are already commercialized or closer to commercialization than other SSEs mentioned in the above sections because of their low cost, potential of mass production, and mechanical flexibility and ductility. As a compromise between the huge number of publications on solid-state polymers and the appropriate presentation here, Figure 9 only shows the most recent research results from 2018 to the present. Most of these results are based on PEO polymers,[136–144] while there are also some reports using other polymer backbones.[145–150] For PEO based polymers, other polymers such as poly(ethylene glycol) (PEG) or solid organics such as succinonitrile (SN) may be applied as additional component. The conductive salt in the polymer structure as complex can be both organic (e.g. sodium bis(fluorosulfonyl) imide (NaFSI), sodium bis (trifluoromethanesulfonylimide) (NaTFSI) or sodium trifluoromethanesulfonate (NaTF)) and inorganic (e.g. $NaClO_4$, $NaPF_6$, and $NaBF_4$). Sometimes other Na-conducting SSEs (for example NaSICONs) have also been applied as the additive to the sodium salts, or even non-Na-conducting solids, like SiO_2, Al_2O_3 or carbon quantum dots (CQDs) were used to increase the conductivity of the solid-state polymers. The mechanism of Na-ion conduction in PEO-Na-salts complexes is explained with enhanced mobility of Na^+ along the polar ether groups within a PEO chain.[151] The beneficial influence of additional other Na-conducting SSEs to increase the conductivity is not clear yet. Although these added Na-conducting SSEs have higher conductivity compared to the solid-state polymers themselves, they should show very limited influence because of their small content and unconnected particles. Moreover, similar effect can also be accomplished even with insulators such as SiO_2, Al_2O_3 and CQDs. The most widely accepted theory is that the formation of space-charge layers between oxide particles and polymer regions is responsible for the enhanced conductivity of the complex.[35] Nevertheless, the limited content of Na-salts in the polymers and longer hopping distance of Na-ions compared to those in crystals result in insufficient conductivity of solid-state polymers

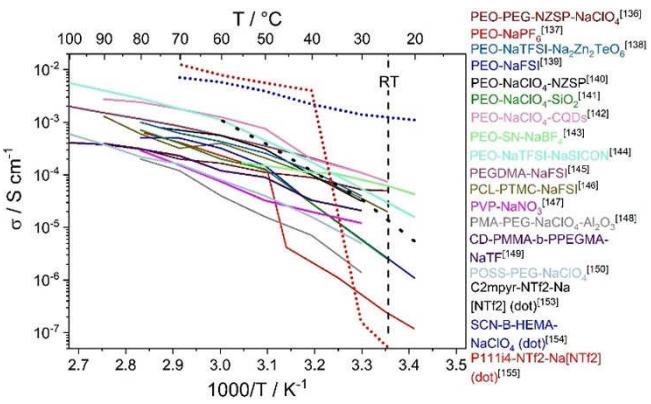

Figure 9. Temperature dependence of the σ_{total} of Na-ion solid-state polymers (solid line) together with plastic crystals (dotted line).

compared to other kinds of Na-conducting SSEs. In Figure 9, even the solid-state polymer with the highest conductivity at RT, PEO-$NaClO_4$-CQDs,[142] only shows a conductivity that barely reached 10^{-4} S cm^{-1}. Solid-state polymers with backbones other than PEO also have similar Na-ion conduction mechanism to PEO-based materials. Figure 9 includes other polymers such as poly(ethylene glycol) methyl ether methacrylate (PEGDMA), polycaprolactone-polytrimethylene carbonate (PCL-PTMC), polyvinyl pyrrolidone (PVP), poly(methacrylate) (PMA), cyclodextrine-multiple oligo(methyl methacrylate)-block-oligo(ethylene glycol) methylether methacrylate (CD-PMMA-b-PPEGMA) and octakis(3-glycidyloxypropyldimethylsiloxy)octasilsesquioxane (POSS). Compared to PEO-based solid-state polymers, their conductivities are not specially higher or lower. The best complex is PEGDMA-NaFSI,[145] which show almost the same conductivity as the best PEO-based complex: PEO-$NaClO_4$-CQDs. Such low conductivity indicates that the SSNBs based on solid-state polymers can hardly be applied at or below RT. Judging from Figure 9, at least about 60 °C is needed to operate the cells based on excellent solid-state polymers, a temperature where they show conductivity of about 10^{-3} S cm^{-1}.

Besides the solid-state polymers which were complexed with conductive salts under dry conditions, organic ionic plastic crystal (OIPC) is also frequently regarded as "solid-state". OIPCs consist of an organic cation-anion pair, like those within an ionic liquid. However, they have regular crystal structures in the solid state. At temperatures below the melting point, an OIPC rearranges to a crystalline phase with lower symmetry through the rotational motion of ions within the long-range ordered lattice. The presence of these rotating ions leads to one or several transitions from orientationally ordered phases to orientationally disordered ones resulting in an increase in entropy with increasing temperature. Thus, eventually these crystals melt with a remarkably low entropy of fusion. A consequence of this structural disorder is the formation of defects (vacancies or extended defects such as dislocations) which enables the motion of ions and hence results in ionic conductivity. These defects also lead to more readily deformable materials, therefore the term plastic crystal.[152] Since OIPCs are supposed to be applied near to their melting point, the definition of "solid-state" is especially tricky to this kind of materials. Three examples are shown in Figure 9. The first one is N-methyl-N-ethyl-pyrrolidinium bis(trifluoromethanesulfonyl) amide (C2mpyr-NTf2) together with sodium bis(trifluoromethanesulfonyl)-amide (Na[NTf2]).[153] The authors clearly claimed that this OIPC is completely solid at temperatures <60 °C. In that case, it can surely be defined as a "solid-state polymer". However, at the same time, it is also clear that C2mpyr-NTf2-Na[NTf2] shows similarly low conductivity as normal solid-state polymers mentioned above. In comparison, although the OIPC of succinonitrile-boron-containing cross-linker 2-hydroxyethyl methacrylate (SCN-B-HEMA)-$NaClO_4$ shows a conductivity higher than 10^{-3} S cm^{-1} at RT,[154] which is also the highest conductivity in Figure 9, (SCN<-B-HEMA)-$NaClO_4$ should be at least partially in liquid phase at >20 °C concluding from the differential scanning calorimetry investigations. In that case, (SCN-B-HEMA)-$NaClO_4$ cannot be defined as "solid-state" according to the definition above. A more representative example is trimethylisobutylphosphonium (P111i4)-NTf2-Na[NTf2].[155] A sharp transition of the conductivity can be found at about 30 °C, where the conductivity strongly increased from 10^{-7} S cm^{-1} to 10^{-3} S cm^{-1} in the temperature range of only 10 °C. The authors attributed this phenomena to the appearance of liquid phase at this temperature. Hence, OIPCs can be regarded as solid-state polymers only in limited compositional and temperature regimes. And as solid-state polymer electrolytes, OIPCs are not especially attractive, because in the solid state they show insufficient conductivity at RT like other solid-state polymers.

2.1.7. Comparison of the Most Conductive Materials

The compositions with the highest σ_{total} in the above mentioned classes of materials are summarized in Figure 10.[13,45,67,94,115,129,156,157] When the satisfactory conductivity criterion of $>10^{-3}$ S cm^{-1} at RT is applied to SSEs as mentioned in Section 2.1, almost all the representative compositions of solid-state sodium conductors fulfill this requirement, indicating the potential of Na-ion-conducting SSEs in general. Specifically, borohydrides and sulfide-based materials show better conductivity compared to oxide-based materials. However, since the σ_{total} of the representative NaSICON and β/β"-alumina both exhibit competitive values compared to the state-of-the-art liquid electrolyte of 1 M $NaClO_4$ in the mixture of ethylene carbonate and dimethyl carbonate (EC-DMC),[156] it can be concluded that the conductivity target for these SSEs has also been achieved. Compared to Li-ion-conducting SSEs, although the Na-ion-conducting SSEs have received much less attention, more outstanding compositions have been developed if only conductivity is considered. $Li_{9.54}Si_{1.74}P_{1.44}S_{11.7}Cl_{0.3}$ possesses the highest σ_{total} among all the Li-ion-conducting SSEs,[13] while two compositions of $Na_{2.88}Sb_{0.88}W_{0.12}S_4$ and $Na_2(CB_9H_{10})(CB_{11}H_{12})$ in Figure 10 exhibit even higher σ_{total}. In addition to the sulfides, the most favored Li-ion-conducting SSEs are $La_3Zr_2Li_7O_{12}$ (LLZ)-based materials, of which $La_3Zr_2Li_{6.55}Ga_{0.15}O_{12}$ is shown in

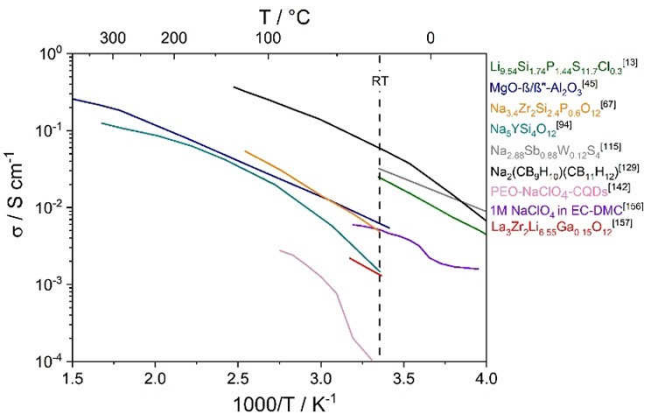

Figure 10. Comparison of the temperature dependence of the σ_{total} of the most conductive Na-ion conductors, together with a liquid electrolyte and a Li-ion conductor.

Figure 10 as a typical example with σ_{total} of 1.3×10^{-3} S cm^{-1} at RT,[157] while almost all classes of Na-ion-conducting materials can satisfy this value (Figure 10). Solid-state polymers are the only exception. In Figure 10, the conductivity of the best solid-state polymer barely reached 10^{-4} S cm^{-1} at RT. Undoubtedly, σ_{total} is not the only decisive parameter for choosing a qualified SSE in SSNB development. Other parameters such as chemical stability, interface compatibility with the electrode, and the design of the cell structure are also important and should receive more attention for materials selection.

It should also be mentioned that all these SSEs are almost electronic insulators. As discussed in the sections above, their σ_e is always lower than 1×10^{-8} S cm^{-1} at RT, which is at least five orders of magnitudes lower than their σ_b. Low σ_e of electrolytes prevents internal leak current in batteries and is the basis of efficient energy storage.

2.2. Stabilities

High conductivity of the SSEs is necessary to obtain high performances of the battery cells. However, apart from the high conductivity, stability of the SSEs is also important for the ultimate commercialization of the SSNBs. SSE stability includes chemical and physical aspects. The chemical stability of the SSEs mainly influences the longevity of the batteries under operating conditions. Specifically, the electrochemical window of the materials influences the choice of the electrode materials and the working voltage of the batteries, affecting, on the one hand, the energy density and, on the other hand, especially the longevity of the batteries under high voltages. The chemical stability of the SSEs in ambient air also influences the longevity and the production processes of the batteries, which may have an impact on the cost of the final product. The thermal stability of the SSEs under a reasonable temperature range decides whether the battery can be operated under practical conditions. The physical stability of the SSEs mainly indicates the mechanical strength of the material, which is important for processing the cells and for the robustness of the cells during application. These aspects are discussed in detail in the following sections.

2.2.1. Electrochemical Window

The electrochemical window of an electrolyte is the voltage range between which the material is neither oxidized nor reduced, i.e. a higher operating voltage oxidizes the electrolyte while a lower operating voltage reduces the electrolyte causing decomposition of the material. A wider electrochemical window of the electrolyte allows more choices for electrode materials, higher energy and power density as well as higher stability during operation. Thus, a wide electrochemical window is beneficial for electrochemical performance and is important for the lifetime of a battery. Generally, SSEs are regarded as more stable since they have a wider electrochemical window compared to conventional liquid electrolytes for both lithium- and sodium-based batteries.[18,42,79] Since electrochemical window is mostly tested or calculated against Na/Na$^+$, it also reflects the stability of the SSEs against Na metal itself.

However, the actual situation may be more complicated.[14] Figure 11 shows the electrochemical stability windows of Na-ion conducting SSEs calculated by thermodynamic principles.[158] In contrast to expectations, the SSEs exhibit relatively small calculated thermodynamic ranges of stability. Referring to the redox potential of Na$^+$/Na, NaSICON is stable between 1.1 and 3.6 V; β-alumina is stable from 0.1 to 3.8 V, but even the simplest Na_3PO_4 is only stable at 0–3.4 V. The situation for sulfides and borohydrides is likely to be worse than for the oxides. The borohydrides mentioned in Section 2.1.5 are not included in the calculation. However, the best borohydride, $Na(BH)_6$ is only stable at 0–3.4 V in the figure. Moreover, the sulfides in Figure 11 all show small electrochemical windows. None of them is stable when the voltage is higher than 2.5 V. The most unstable composition, Na_3SbS_4, has an electrochemical window as narrow as 0.1 V (1.8–1.9 V vs. Na/Na$^+$). For comparison, the practical electrochemical window of the state-of-the-art liquid Na-ion-conducting electrolytes is mostly 0–4 V or better,[39] while that of polymer based electrolytes (including both gel-polymers and solid-state polymers) is even better (0–4.5 V or better).[35] In the above analysis, the thermodynamic limit is calculated as the voltage (the Na chemical potential) at which the electrolyte is expected to decompose into other phases, accompanied by Na extraction. Such decomposition into distinct phases may not always be possible at RT until a sufficient driving force for the reaction is reached at higher potentials, which can be understood as a kinetic barrier.[158] Scale bars on partial compositions of Figure 11 show their kinetic upper limit. As anticipated, the predicted kinetic voltage limit is always higher than the thermodynamic limit. Some of the compositions show huge differences, e.g. Na_3SbS_4 and $NaBH_4$. However, it should be emphasized that Figure 11 is still completely based on theoretical calculations. The actual situation might be very different during practical applications because of the formation of solid-solid interfaces. For example, although the electrochemical window for Na_3SbS_4 is only 0.1 V as calculated thermodynamically, with 1.4 V as the calculated kinetic threshold, Wang *et al.* reported an electrochemical

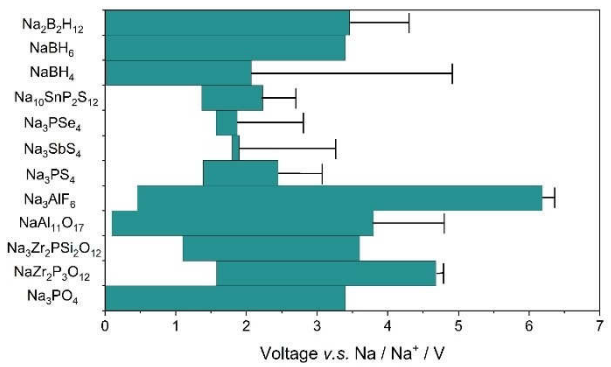

Figure 11. Thermodynamically calculated electrochemical stability windows of Na-ion conducting SSEs. Error bars right to the stability regions (thick bars) indicate their calculated kinetic upper limit for oxidation.

stability of 0–5 V for Na_3SbS_4 with cyclic voltammetry (CV) measurements of a Na/Na_3SbS_4/Pt cell (although a very tiny signal can be observed in the plot at about 1 V).[112] Similarly, some other Na-ion-conducting SSEs also display higher electrochemical stability compared to the calculated value in Figure 11, as shown in Table 2. So far no detailed research has explained the mismatch between the calculated and experimental electrochemical window. However, some explanations can be put forward. Firstly, when SSE materials are in contact with sodium metal, a passivating reaction may take place at the interface. With the formation of such a protective layer, even if possibly only a thin nanolayer, a further reaction is prevented. Due to the passivating layer, the practical electrochemical window may also be widened compared to the calculated values, because the calculation does not take a third material into consideration. Secondly, unlike the homogeneous system of a liquid electrolyte, secondary phases may exist within the SSEs, especially at the surface of the materials because of contact with the ambient environment, e.g. contact with ambient air during sintering for oxide-based SSEs. These secondary phases may also act as a protective layer for the SSEs and widen the electrochemical window during testing. Thirdly, even if the decomposition reaction takes place both thermodynamically and kinetically when the operating voltage is higher than the limit, it should still be taken into consideration that the decomposition reaction may show very moderate influence to cell-performance even until the longevity of the cells. For example, in Table 2, both $Na_{3.1}Zr_{1.95}Mg_{0.05}Si_2PO_{12}$ and $Na_4(B_{12}H_{12})(B_{10}H_{10})$ show a very slight oxidation peak during the CV measurements. In general, such oxidation indicates the start of the decomposition reaction and should be regarded as the limit of the electrochemical window. However, since the scan rates are very slow (0.1 $mV\,S^{-1}$) and the height of the peaks is very low (in $nA\,cm^{-2}$ level), the actual decomposition can be extremely slow. As long as the decomposition reaction has no obvious influence on the performance of the battery during its longevity (normally >1000 cycles), it can still be considered that the SSEs can be applied even beyond the limit of the electrochemical window. However, further experiments are needed to support this point. Instead, although Na_3PS_4 and Na_3SbS_4 both show a stable electrochemical window between 0 and 5 V (Table 2), the scan rate in their CV measurement is extremely high (5 $mV\,S^{-1}$). In that case, the oxidation peak might be suppressed for kinetic reasons, and the conclusion of "stable electrochemical window of 0 to 5 V" might be inappropriate. The final evaluation should still rely on a full cell operated under practical parameters as listed in Table 1. Unfortunately, no such published data are currently available.

2.2.2. Stability in Ambient Air

The stability in ambient air of SSEs is mainly related to the processing of the batteries. The investment costs and consumables for the SSE processing of air-sensitive or air-insensitive materials is very different, while low-cost processing is of great significance for battery production. Thus, it is necessary to understand the stability of the SSEs in contact with ambient air, which is discussed in the following.

In general, the commonly held opinion is that oxide-based SSEs show negligible reactions with ambient air compared to other chalcogenides or hydrides because they are normally produced by sintering in air. However, in the field of SSLBs this topic has attracted considerable attention due to the intensively studied Li-ion-conducting oxides such as LLZ-based SSEs, which react with H_2O and CO_2 in ambient air and form thick blocking layers on the surface.[160] In the case of NaSICON-type oxides, they are also considered to form tiny surface layers of hydroxides and carbonates during long-term exposure in ambient air because of their reactivity to H_2O and CO_2.[161–163] However, no study clearly reveals that such reactions take place with the NaSICON-phase themselves or with secondary phases existing on the surface or at the grain boundaries of the materials. Indeed, discussions tend towards the latter view, namely that trace amounts of salts such as Na_3PO_4 on the surface or along the grain boundaries absorb H_2O and CO_2 from the ambient air. Similarly, the uptake of H_2O and CO_2 by β/β″-aluminas was confirmed a long time ago,[164–166] also resulting in compounds such as NaOH or Na_2CO_3. The difference to NaSICONs is the reaction mechanism, i.e. the reaction is generally regarded as a direct interaction with the β/β″-aluminas themselves, also leading to an ion exchange of Na^+ by H_3O^+ in the conduction planes.[164–166] It should be mentioned that the reaction conditions in the above references are quite severe, e.g. long contacting times ranging from days to months, direct soaking of the samples in water or even acid/alkaline solutions and increased temperature. The influence on conductivity of the materials was moderate. Generally speaking, when handled with care, it is not very difficult to process batteries with oxide-based SSEs.

It can be expected that the stability of Na-ion-conducing SSEs based on sulfides raises more concerns, because lithium sulfides are very sensitive to the moisture in ambient air

Table 2. Electrochemical window tested by CV measurements for different Na-ion conducting SSEs.

Category	Composition	Scan rate [$mV\,s^{-1}$]	Electrochemical window (V, *v.s.* Na/Na^+)	Comments	Ref.
NaSICON	$Na_{3.1}Zr_{1.95}Mg_{0.05}Si_2PO_{12}$	0.1	0–9	Slight oxidation peak found at 4.3 V	[77]
	$Na_{3.4}Sc_{0.4}Zr_2Si_2PO_{12}$	0.1	0–6	–	[48]
Sulfide	Na_3PS_4	5.0	0–5	Very fast scan rate	[10]
	Na_3SbS_4	5.0	0–5	Very fast scan rate	[112]
Borane	$Na_4(B_{12}H_{12})(B_{10}H_{10})$	0.1	0–6.5	Slight oxidation peak found at 3 V	[133]
Solid-state polymer	PEO-$NaPF_6$	0.1	0–5	–	[159]

resulting in poisonous H_2S as one of the products,[160] which is not only harmful for cell performance, but can also be dangerous for users. Similar conclusions can be associated with sodium-based sulfides because of the very similar properties of lithium and sodium compounds. Shang et al. also discussed the reaction between $Na_3P_{1-x}As_xS_4$ and H_2O in detail and confirmed the sensitivity of H_2S production.[167] Information on the reactivity of sulfide-based sodium compounds to oxygen is less definite. Although it is stated that sulfide SSEs containing phosphorus are not only sensitive to moisture in air, but also in the presence of oxygen,[113,126] no experimental support was found to prove the point. Banerjee et al. confirmed that exposing Na_3PS_4 in dry air results in the secondary phase formation observed in the XRD pattern.[126] However, the reflections of the secondary phases were defined as "unknown". Further experiments are necessary to clarify the point. It is worth mentioning that several references claimed that Na_3SbS_4 -based materials are stable in ambient air.[112,113,115,126,168] Wang et al. discussed the XRD patterns and Raman spectra of Na_3SbS_4 before and after exposure in air. They found that Na_3SbS_4 will only form $Na_3SbS_4 \cdot 9H_2O$ after contact with moisture in air,[112] which can be dehydrated backwards to Na_3SbS_4 after heating up to 150 °C in vacuum. No H_2S production was found in the process, which is confirmed by other reports.[113,115,126] Tian et al. pointed out that air treatment even improves the stability of the Na_3SbS_4 electrolyte-Na metal interface upon electrochemical cycling because the formation of a newly discovered hydrate phase, $Na_3SbS_4 \cdot 8\ H_2O$, led to the generation of desired passivating products (i.e. NaH and Na_2O) at the interface, which suppressed the electrolyte decomposition.[168] Kim et al. and Banerjee et al. managed to produce Na_3SbS_4 from aqueous solution.[113,126] The high stability of Na_3SbS_4 with respect to moisture is explained by the strong bonding of the Sb^{5+} (soft acid) to the S^{2-} ions (soft base) allowing the Na_3SbS_4 to retain its chemical stability in an ambient environment.[112] However, the formation of $Na_3SbS_4 \cdot 9H_2O$, although harmless, is still very detrimental to the performance of the material, because the conductivity of $Na_3SbS_4 \cdot 9H_2O$ is more than three orders of magnitude lower than that of Na_3SbS_4 at RT.[112] Therefore contact with moisture has to be prevented during processing of the material. Since the development of Na-ion-conducting SSNBs is still at an early stage, no information on the stability in air of other sulfides (or chalcogenides) is yet available.

After the discovery of borohydrides as possible Na-ion conductors at RT, hardly any work has been devoted to the stability of the materials in ambient air. On the one hand, borohydrides are a relatively "novel" category of Na-ion-conducting SSEs, and, on the other hand, earlier investigations confirmed the chemical stability of borohydrides (or carba-borohydrides) in ambient air or even in water solution.[169,170] It is known that $B_{10}H_{10}^{2-}$ and $B_{12}H_{12}^{2-}$-based salts do not only exist in aqueous solution, but also have high stability in strong acidic or basic solutions.[169] The chemical stability of $CB_{11}H_{12}^{-}$-based salts with respect to miscellaneous solutions including water is also confirmed.[170] Moreover, in the discussion of the conductivity of $Na(CB_9H_{10})$ and $Na(CB_{11}H_{12})$, although Tang et al. did not specifically discuss the chemical stability of the materials in ambient air, it is clear that these materials are prepared directly out of water solutions,[129,132] indicating their stabilities with respect to water and air. Although Udovic et al. mentioned possible hygroscopic properties for borohydrides,[130] the uptake of water can be reversed by drying. The materials can still be regarded as air-stable at room temperature.

Although the main backbone of solid-state polymers, PEO, is stable in air, as well as the inorganic salts like $NaClO_4$, $NaPF_6$ etc., they all largely absorb water from the ambient air. Water contained solid-state polymer may cause battery-bulge because of the water-decomposition during charge and discharge. The advantage of these materials is that the absorption is reversible. The absorbed water can be removed by heat or vacuum. It should be noticed that some organic sodium salts, like NaFSI may be oxidized in air irreversibly. Special attention should be taken to these materials.

In brief, although the related research is still in progress, it can already be concluded that Na-ion-conducting SSEs are slightly sensitive to moisture and CO_2. Compared to oxides and borohydrides, sulfide-based Na-ion-conducing SSEs are more problematic in contact with ambient air. Nevertheless, it seems that the hygroscopicity of most of the Na-ion-conducing SSEs can be solved simply by making use of a drying room during practical applications.

2.2.3. Thermal Stability

The thermal stability of Na-ion-conducting SSEs is taken into consideration because this is a well-known problem for state-of-the-art Li-ion or Na-ion LBEs.[79,160,171–173] They tend to exhibit battery failure or thermal runaway at temperatures > 100 °C mainly due to the decomposition of the materials. Such temperatures are easily reached and may lead to failure because of high-power applications, complications of the operating environment (such as temperature change and possible mechanical impact on the device), abuse of the devices etc.. For the Na-ion conducting SSEs discussed in the current study, such a problem is comparatively easy to remedy. The oxide-based materials, either NaSICONs, β/β"-alumina or $Na_5LnSi_4O_{12}$, all have decomposition temperatures of > 1000 °C. All these materials also need processing temperatures of $>$ 1000 °C to achieve phase-pure and dense bodies.[44,67,95] The sulfide-based materials, although less robust compared to the oxides, also need a sintering procedure with a temperature of about 300 °C and are thermally stable up to this temperature.[10,115,117,119] It should be noted that the thermal stability of the sulfides discussed here refers to stability in protective atmospheres such as dry Ar, while that of the oxides refers to ambient air. Because sulfides react readily with water (at RT) or oxygen (when heating up), the gas-tightness of sulfide batteries must be of a sufficient quality to avoid decomposition. The thermal stabilities of borohydride-based Na-ion-conducting SSEs are less well understood compared to the above two classes of materials. So far, $B_{10}H_{10}^{2-}$ and $B_{12}H_{12}^{2-}$-based salts are known to have thermal stability up to 300 °C when the oxygen partial pressure is low (vacuum or Ar),[133] whereas the stability

limit of $CB_9H_{10}^-$ and $CB_{11}H_{12}^-$-based salts is not well established. However, at least 200 °C is still a safe temperature in vacuum or Ar.[129] Solid-state polymers also possess higher thermal stability compared LBEs since no liquid phase is involved. As the major category in solid-state polymers, PEO-based solid-state polymers are thermally stable up to temperatures of 200–300 °C.[35] Generally speaking, oxides have better thermal stability compared to sulfides, boron hydrides and solid-state polymers, while these SSEs are almost all better than the state-of-the-art LBEs in Li-ion or Na-ion batteries.

It should also be mentioned that, although normally thermal stability indicates the stability of the material at high temperatures where decomposition starts, for SSEs behavior at temperatures below RT should also be addressed because they normally have a higher activation energy compared to the state-of-the-art LBEs resulting in a faster decrease of conductivity with decreasing temperature. For applications under severe ambient conditions with low temperatures, battery failure may take place because the conductivity of the SSEs is too low. Figure 12 shows the σ_{total} of some representative Na-ion-conducting SSEs.[60,64,67,115,116,129,133] At −20 °C, all SSEs in Figure 12 have a universal decrease of σ_{total} of about 1–2 orders of magnitude compared to conductivity at RT. When the upper requirement for SSEs of $> 10^{-3}$ S cm^{-1} is applied at −20 °C, only the two best SSEs of $Na_{2.88}Sb_{0.88}W_{0.12}S_4$ and $Na_2(CB_9H_{10})(CB_{11}H_{12})$ are qualified. However, since the aim of this discussion is only to avoid battery failure, the lower limit of $> 10^{-4}$ S cm^{-1} should be sufficient to keep the battery alive. In that case, a relatively large number of oxides, sulfides and borohydrides can reach this level. In Figure 12 only $Na_4(B_{10}H_{10})(B_{12}H_{12})$ shows a conductivity of 10^{-5} S cm^{-1} at −20 °C because of the very high activation energy. In summary, it can be concluded that Na-ion-conducting SSEs do not cause any problems with respect to battery failure due to too low σ_{total} at low temperatures as long as proper compositions are chosen.

2.2.4. Mechanical Stability

As an example of commercialized Li-ion batteries, the mechanical stability of an 18650 battery is not based on key battery materials such as the anode, cathode or electrolyte, but on the container material, which in most cases is aluminum. This is easy to understand because the cell materials of the liquid-electrolyte-based 18650 battery do not have significant mechanical strength and have to be stabilized by the aluminum case. For an 18650 battery, the failure force is several kN both under axial and transverse compression.[174,175] Because of the current early stage of SSNB development, it is difficult to discuss their mechanical stability in a coordinated manner. There is no full battery design even close to practical application. The size and outer shape of a potential commercialized cell are still unknown. What kind of casing should be applied is also unknown. Since the SSNBs reported on the laboratory scale are mainly based on button-cell designs with an SSE as support, at this point only the mechanical properties of SSEs can be used for comparison. Even if only this information is considered, related investigations on mechanical properties are completely insufficient. With respect to the most important parameter for the evaluation of the mechanical stability of a material under practical applications, Nonemacher et al.[176] and Sheng et al.[89] investigated the fracture toughness of Al_2O_3-Y_2O_3-substituted NaSICON and ZrO_2-substitued β/β"-alumina resulting in fracture toughness values of 1–2 and 2–3 MPa m$^{0.5}$, respectively. For comparison, the aluminum casing of the 18650 battery has a fracture toughness of about 20 MPa m$^{0.5}$. Such a comparison, although rough, indicates the problem of brittleness for oxide-based SSEs. A similar comparison for sulfides and boranes is not possible because of the lack of data. However, as mentioned in Section 1 (Introduction), SSNBs are mainly being developed for stationary applications, which require lower mechanical stability compared to mobile applications because of the low probability of mechanical impact from the environment.

Because of the mechanical flexibility and ductility of polymers, the above parameters are not suitable to evaluate solid-state polymers. The mechanical stability of polymers are frequently expressed by tensile strength and compressive strength, where PEO based polymers normally have tensile strength of about 1 MPa, and compressive strength of about 10 MPa.[35,138,142,149] Since polymers (gel-polymer) have already been commercialized and applied in the devices like cellphones, the mechanical stability of polymer based electrolytes is generally believed to be trouble-free.

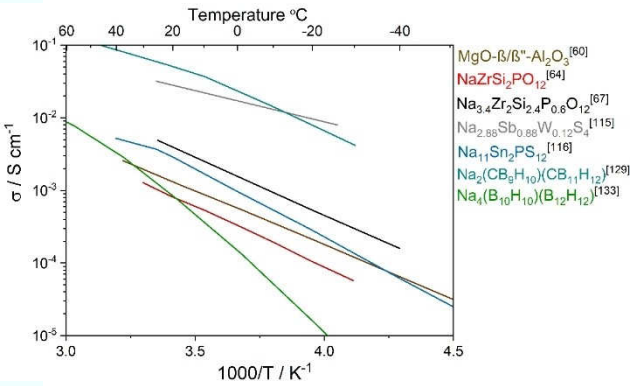

Figure 12. Comparison of the temperature dependence of the σ_{total} of different Na-ion conducting SSEs at low temperatures.

2.3. Compatibility with Na Metal

The compatibility of Na-ion-conducting SSEs with Na metal is above all related to the reactivity between SSEs and Na metal, which is defined by the electrochemical stability windows of Na-ion-conducting SSEs, as described in Section 2.2.1. However, a passivating layer or secondary phase between SSEs and Na metal may stop the decomposition of SSEs. As long as such interface reactions do not penetrate the SSE, this may widen the application window for SSEs. However, the reactivity between SSEs and Na metal is just one aspect related to compatibility. Other parameters such as interface resistance and dendrite tolerance, are also important for practical cell

operation. Ultimately, the most direct method to fully evaluate the compatibility between SSEs and Na metal is the practical test of Na/SSE/Na symmetric cells. All the parameters related to the compatibility can be inspected by the cell operation, including interface stability with Na-metal, dendrite tolerance, internal resistance, etc. When all the parameters for compatibility are satisfactory, the criterion of an areal capacity of $\geq 3\ mAh\ cm^{-2}$ (per half cycle, e.g. a plating or stripping of the metal electrode) at a current density of $\geq 1\ mA\ cm^{-2}$ is fully satisfied.[15,181] When the key parameters of the commercial 18650 batteries (Table 1) are also applied here, the total areal capacity of the symmetric cells during the whole operating longevity should be over 6000 $mAh\ cm^{-2}$ since the cells should survive for at least 1000 cycles, and the interface resistance of the cells should be at least $< 20\ \Omega\ cm^2$.

Fortunately, several symmetric cells have already been tested in earlier publications which display performances that can be compared with the above criteria, as listed in Table 3. From these symmetric cells, the following points can be extracted and discussed. Firstly, in general, current symmetric cells still cannot fulfill the criteria of practical application. However, some of the cells have already been partially qualified. For example, a $Na_{3.4}Zr_2Si_{2.4}P_{0.6}O_{12}$ and a β″-Al_2O_3-based symmetric cell both show interface resistance as low as 4 and 8 $\Omega\ cm^2$ at RT, respectively, indicating trouble-free interfaces between Na metal and the SSEs.[67,93] These very new results from 2019 reveal a considerable improvement compared to earlier reports, the majority of which specify hundreds or dozens of $\Omega\ cm^2$ thus indicating ongoing developments in this field. Some β″-Al_2O_3 -based samples also display a high operating current density (0.5–5.5 $mA\ cm^{-2}$) and areal capacity per half cycle (3 $mAh\ cm^{-2}$) at RT.[93] Although no cell in Table 3 reached a total areal capacity of $> 6000\ mAh\ cm^{-2}$, one of the $Na_3Zr_2Si_2PO_{12}$-based samples did reach quite a high level of 1000 $mAh\ cm^{-2}$.[179] There is still potential for the improvement of SSNBs. It should also be mentioned that the dendrite growth of Na metal is regarded as the major failure mode of symmetric SSNBs,[182] which is similar to that of SSLBs.[14,183] Although most of the reports in Table 3 did not mention how their cells finally failed, dendrite formation is probably the main reason. This is currently the major obstacle that prevents symmetric SSNBs from satisfying the requirements for practical application.

Secondly, although sulfides and boranes generally show better conductivity compared to oxides (see Figure 10), at the symmetric cell level, their development is not as mature as that of the oxides. In Table 3, there is generally no data on their interface resistance, and their current density and areal capacity during testing are also inferior compared to the oxide-based cells. Although interface resistance and dimension data are missing in sulfide- and borane-based cells in Table 3, the total resistance of the cells can be obtained from the results of galvanostatic cycling, where the total resistance of Na_3PS_{4-} and Na_3PSe_4-based cells is as high as 5000 and 2000 $\Omega\ cm^2$, respectively.[118,180] In view of the sufficient conductivity of these two materials (see Figure 7), such high total resistance of the symmetric cells should mainly come from the interface between the Na metal and the respective SSE. The Na_3SbS_4-based symmetric cell has a total resistance of about 500 $\Omega\ cm^2$,[112] which is on the moderate level in Table 3, but still much higher than the practical application level (see Table 1). The most interesting result is shown by a $Na_4(B_{12}H_{12})(B_{10}H_{10})$-based cell, where the total resistance is only about 10 $\Omega\ cm^2$, indicating both good conductivity of the material itself and good interface conditions between the material and Na metal. The only problem is that the data were obtained at 60 °C instead of RT, and there are no RT data available for any borane-based symmetric cell. Moreover, although $CB_9H_{10}^-$ or $CB_{11}H_{12}^-$ salts show the highest σ_{total} of all the Na-ion-conducting SSEs (Figure 10), no symmetric cell has been reported to date, indicating the early stages of development. Finally, although

Table 3. Performances of different Na/SSE/Na based symmetric cells.

Category	Composition of SSE	Interface resistance [$\Omega\ cm^2$]	Current density [$mA\ cm^{-2}$]	Areal capacity per half cycle [$mAh\ cm^{-2}$]	Total areal capacity [$mAh\ cm^{-2}$]	Temp. [°C]	Ref.
NASICON	$Na_3Zr_2Si_2PO_{12}$	400	0.15–0.25	0.15–0.25	105	65	[177]
	$Na_{3.2}Zr_{1.9}Ca_{0.1}Si_2PO_{12}$	175	0.1–0.3	0.1–0.3	150	RT	[178]
	$Na_{3.4}Zr_2Si_{2.4}P_{0.6}O_{12}$	4	0.6	1.8	180	RT	[67]
	$Na_3Zr_2Si_2PO_{12}$ coated with graphene	46	1	1	1000	RT	[179]
Beta alumina	β″-Al_2O_3	150	0.1	0.05	100	58	[91]
	TiO_2-β″-Al_2O_3	–	0.044	0.006	0.073	RT	[92]
	β″-Al_2O_3	8	0.5–5.5	3.0	33	RT	[93]
Sulfide	Na_3PS_4	–	0.1	0.1	10	RT	[180]
	Na_3PSe_4	–	0.025	0.013	0.25	RT	[118]
	Na_3SbS_4	–	0.1	0.05	8.3	RT	[112]
Borane	$Na_4(B_{12}H_{12})$ $(B_{10}H_{10})$	–	0.1	1.2	28.8	60	[133]
Solid-state polymer	PEO-NZSP-$NaClO_4$	–	0.2	0.2	56	55	[136]
	PEO-$NaPF_6$	–	0.1	0.1	10	80	[137]
	PEO-$Na_2Zn_2TeO_6$	47	0.1	0.05	15	80	[138]
	PEO-NaSFI (Na with C as electrodes)	–	0.3	0.15	240	80	[139]
	PEO-$NaClO_4$-$Na_3Zr_2Si_2PO_{12}$	–	1.0	1.0	500	60	[140]
	PEO-CQDs-$NaClO_4$	–	0.05–0.1	0.05–0.1	9	60	[142]
	PEGDMA-NaFSI	–	0.1	0.1	80	60	[145]
	POSS-PEG-$NaClO_4$	–	0.5	0.5	1775	80	[150]

the number of reported symmetric SSNBs is smaller than their lithium counterparts, the performance of the symmetric SSNBs is already very promising. As a very representative example, Sharafi et al. reported a symmetric SSLB based on Na/LLZ/Na, which had an interface resistance of 2 $\Omega\,cm^2$, current density of 0.2 $mA\,cm^{-2}$, areal capacity of 0.2 $mAh\,cm^{-2}$ per half cycle, and total areal capacity of 40 $mAh\,cm^{-2}$, all measured at RT.[184] Although the interface resistance is better than any cell in Table 3, the cycling performances are inferior compared to those in Table 3. As mentioned above, the failure of the cycling of SSLBs and SSNBs is mainly due to dendrite formation. There are two possible reasons for the higher dendrite tolerance of SSNBs compared to SSLBs. Firstly, sodium atoms in sodium metal have a higher self-diffusion coefficient compared to that of lithium atoms in lithium metal,[185,186] and the difference is as high as about 100 times. A higher self-diffusion coefficient results in higher dendrite tolerance.[187] Secondly, benefitting from the larger size of Na atom/Na ion compared to that of Li atom/Li ion, the penetration effect of Na atom/Na ion is also weaker than that of Li atom/Li ion, resulting in higher dendrite tolerance.

Apparently the database of symmetric cells based on solid-state polymer is more abundant compared to other categories, because of their low cost, facilitation of mass production, mechanical flexibility and ductility, as well as their popularity as a result. Their performances are not especially different from other kind of SSEs. The only difference is symmetric cells based on solid-state polymer can only be operated at enhanced temperatures instead of RT. The insufficient conductivity at RT is surely the reason. Under the actual operation temperature of these symmetric cells, the conductivity of the solid-state polymers is about $10^{-3}\,S\,cm^{-1}$, which is close to other SSEs under RT. Generally, at the present stage the starting point of SSNB-development gives clear perspectives for successful performance improvements.

2.4. Existing Full SSNBs

For evaluation of a full battery, the C-rate is a preferred general parameter, where nC means the battery is fully charged/discharged at a constant current in $\frac{1}{n}$ hours. This C-rate test is favorable because it clearly indicates how fast the whole active material for energy storage can be fully charged or discharged. However, in tests with solid-state batteries the current density ($mA\,cm^{-2}$) is often used for comparisons. As an example, NVP was frequently applied in SSNBs as a cathode material. When it is operated under typical test conditions in publications, i.e. 1 C with mass loading of 1 $mg\,cm^{-2}$, the actual current density is 0.12 $mA\,cm^{-2}$. In comparison to the standard of 18650 cells (1 C indicates ~5 $mA\,cm^{-2}$, see Table 1), the value is much too low. If the current density of 5 $mA\,cm^{-2}$ should be reached under the same C-rate, theoretically at least 40 $mg\,cm^{-2}$ of mass loading should be applied for NVP-based SSNBs. Unfortunately, to date this is very challenging because much thicker cathode layer as well as much higher content of active materials in cathode layer have to be applied, which brings many difficulties like increased internal resistance, longer distance for Na-ion diffusion, engineering problems and so on. Until now, no publication of any SSNB even reported a value close to such mass loading. Similarly, the specific capacity ($mAh\,g^{-1}$) is an academic-preferred unit for energy density, indicating the capacity of a battery per unit weight of the active material for energy storage. However, the high specific capacity in academic research is not necessarily reproduced when the battery is developed towards practical applications because of the large difference of mass loading. These two issues are the actual technological gaps between academic research of solid-state batteries and practical application. The ultimate goal of practical application for a battery is the high gravimetric energy density, which is expressed by the unit of $Wh\,kg^{-1}$, indicating the total energy storage of the battery device per weight unit of the device. 18650 batteries typically have energy densities of 150–250 $Wh\,kg^{-1}$ (Table 1). However, to date there is no report which notes the weight of the full SSNB device, not even the summation of the weight of the anode, cathode and electrolyte of the cells. Therefore, it is difficult to obtain statistics on the gravimetric energy density of the published SSNBs, which also indicates the early development stage of SSNBs. Nevertheless, almost all reports on SSNB full cells mention the areal capacity of the cell, which can be used as a criterion to compare them with 18650 cells instead of the gravimetric energy density, which, as derived from Table 1, is about 3–6 $mAh\,cm^{-2}$. In addition, as mentioned in Section 2.3, some reports agree on the criterion of areal capacity of $\geq 3\,mAh\,cm^{-2}$ (per half cycle, e.g. a plating or stripping of the metal electrode) at a current density of $\geq 1\,mA\,cm^{-2}$,[15,181] which can be applied as the starting point for the present discussion.

Table 4 shows the performance of different SSNB full cells. For illustration, some SSNB full cells containing small amounts of LBE are also listed. Above all, no cell fulfilled the criterion, and most of the reported cells deviate by over one order of magnitude, not only for areal capacity, but also for current density. Moreover, more than 1000 cycles have also hardly been reached. In general, for the SSNBs based on oxide SSEs, the performance of the full cells is obviously weaker than that of the symmetric cells (see Table 3), either judging by the current density or by the areal capacity. Since the main difference between the full cell and half-cell is the additional interface between cathode and SSE, it can be reasonably concluded that this interface is the bottleneck for performance. The possible reason for this bottleneck is often insufficient contacts between randomly arranged grains of SSEs and electrode active materials leading to highly resistive ion-conduction paths and a limited electrochemical reaction. The rigid contacts between SSEs and electrode active materials are further damaged by the volume change of electrode active materials during electrochemical cycling.[14,189] Similar difficulties are also found for SSLBs.[43] Nevertheless, when the interface between the solid-state cathode and electrolyte is in contact with an added LBE, the cycling performance shows an apparent improvement (Table 4),[72,189] because ionic transport can bypass the poorly permeable rigid interface. The volume change of cathode active materials during electrochemical cycling can be absorbed by

Table 4. Performances of different SSNB full cells, including LBE-assisted SSNB full cells.

Cell components	Electrode area [cm^2]	Current density [$mA\ cm^{-2}$]	Areal capacity [$mAh\ cm^{-2}$]	Longevity (cycle numbers)	Degradation [%]	Temp. [°C]	Ref.
$Na_3V_2P_3O_{12}$ | NZSP coated with graphene | Na	~0.8	0.018	0.18	30	14	80	[179]
$Na_3V_2P_3O_{12}$ | liquid electrolyte | NZSP coated with graphene | Na	~0.8	0.18	0.18	300	15	RT	[179]
$Na_3V_2P_3O_{12}$ | La-substituted NZSP | Na	1	~0.02	~0.2	40	33	80	[72]
$Na_3V_2P_3O_{12}$ | ionic liquid | La-substituted NZSP | Na	1	1.5	0.15	10000	~0	RT	[72]
Na_xCoO_2 (0.8 μm thin film) | Sc-substituted NZSP | Na	0.8	0.008	0.05	100	25	RT	[188]
Infiltrated $Na_3V_2P_3O_{12}$ | $Na_{3.4}Zr_2Si_{2.4}P_{0.6}O_{12}$ | Na	0.8	0.035	0.35	100	9	RT	[189]
Infiltrated $Na_3V_2P_3O_{12}$ | $Na_{3.4}Zr_2Si_{2.4}P_{0.6}O_{12}$ | Na	0.8	0.13	0.2	100	9	RT	[189]
Na_xCoO2 (0.7 μm thin film) | β"-Al_2O_3 | Na	0.25	0.004	0.011	40	27	RT	[190]
Na_2O-Fe_2O_3-P_2O_5 glass | β"-Al_2O_3 | Na	1.1	0.005	0.05	600	15	30	[191]
$Na_3V_2P_3O_{12}$ in polymer | Carbon coated β"-Al_2O_3 | Na	1.1	0.07	0.35	100	10	58	[91]
TiS_2 | Na_3PS_4 | Na-Sn	0.8	0.013	1.3	10	5	RT	[10]
$NaCrO_2$ | Na_3PS_4 | Na-Sn	0.8	0.013	–	20	33	RT	[111]
FeS_2 | Na_3PS_4 | Na-Sn	0.8	0.15	0.7	100	18	RT	[180]
$NaCrO_2$ | Na_3SdS_4 | Na-Sn	1.3	0.05	1	1	–	30	[126]
FeS_2 | Na_3SdS_4 | Na-Sn	1.3	0.05	1.1	50	38	30	[113]
$NaCrO_2$ | $Na_4(B_{12}H_{12})$ $(B_{10}H_{10})$ | Na	1.1	0.034	0.17	250	15	RT	[192]
$Na_{0.67}Ni_{0.33}Mn_{0.67}O_2$-C-polymer | PEO-NZSP-$NaClO_4$ | Na	3.1	~0.025–~0.33	~0.25	35	7	55	[136]
NVP-C-polymer | PEO-$NaPF_6$ | Na	0.5	0.56	0.28	200	14	80	[137]
NVP-C-polymer | PEO-$Na_2Zn_2TeO_6$ | Na	~1	0.04	0.21	100	6.6	80	[138]
NVP-C-Polymer | PEO-NaFSI | Na-C	0.36	3.1	0.78	10000	35	80	[139]
$Na_2MnFe(CN)_6$-C-PEO | PEO-$NaClO_4$-$Na_3Zr_2Si_2PO_{12}$ | Na	0.38	0.19	0.37	300	17	60	[140]
NVP-C-polymer | PEO-CQDs-$NaClO_4$ | Na	–	0.21	0.21	100	12	60	[142]
NVP-C-polymer | PEGDMA-NaFSI | Na	–	0.11	0.22	925	13	60	[145]
$Na_xV_2O_5$-C-polymer | POSS-PEG-$NaClO_4$ | Na	0.28	0.04	0.16	50	50	80	[150]

the "soft" interlayer of LBE. An advanced thin-film fabrication technique was also applied to improve the situation,[188,190] because in the case of a very thin cathode layer, the endurance of SSEs with respect to the volume change of cathode active materials during cycling is also higher. However, this strategy is unfavorable for practical applications due to the high cost of the advanced thin-film fabrication technique and limited effective electrode active materials. When SSNBs without LBE are discussed, and also no advanced thin-film fabrication technique is applied, the high interface resistance between cathode and electrolyte can also be reduced by a smart electrode design, as reported by Lan et al. and shown in Figure 13.[189] In the design, instead of the traditional cathode fabrication by mechanical mixing and sintering of SSE and cathode active materials, the cathode active material is prepared in situ on the pore walls of the porous SSE backbone. Such a design improves the solid-state electrode/electrolyte contact as effective as the electrode/liquid electrolyte, provides effective ion exchange and minimizes the stress caused by the dimensional change of electrode active materials during charging and discharging processes. The performances of the cells, although still lower than required, are competitive with all oxide-based SSNBs. Despite this achievement, sulfide-based SSNBs still show the best performance so far (Table 4).

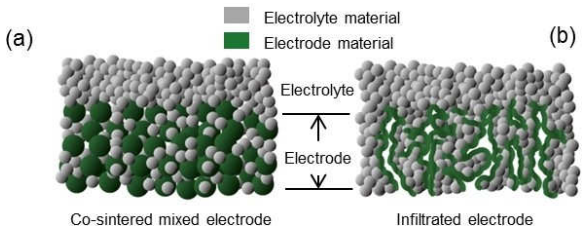

Figure 13. Sketches of different electrode structures: a) mixed and sintered electrode; b) infiltration electrode. Reprinted with permission from Ref. [189] (Copyright 2019, Elsevier Ltd.).

Especially with respect to areal capacity, the data reported in Table 4 for sulfide-based SSNBs are hard to achieve for any other type of SSEs and are promising even compared with the practical application level of $\geq 3\ mAh\ cm^{-2}$. The most likely reason is the rubber-like mechanical behavior of sulfides instead of the stiffness of oxide ceramics. This property decreases the interface problem, as mentioned above for oxide-based SSEs. The main problem of sulfide-based SSNBs is the current density, which is not superior to other SSEs nor is it close to the level required for practical applications ($\geq 1\ mA\ cm^{-2}$). The high internal resistance due to the inappropriate cell design of electrodes and SSEs might be the reason for the low current density, as mentioned in Section 2.3. Finally, the borane-based

SSNB full cells are still at an early stage of development in comparison to the SSNBs of the two other types of SSEs. Only one cell is listed in Table 4,[192] which is not enough to draw definite conclusions. However, the reported borane-based SSNB shows at least an average performance, indicating the potential of the system. Similar to the symmetric cells, solid-state polymer-based cells are more often described in publications than cells of other kinds of SSEs, indicating their popularity and easiness of assembling. Their performance is also remarkable. Zhao et al.[139] operated their cell at 3.1 mA cm^{-2} for 10000 cycles. The reason of the long-term stability is similar to sulfide-based SSNBs, where the soft interfaces between electrolyte and cathode are beneficial for the electrochemical operation. The main disadvantage for solid-state polymer-based cells is that they cannot be operated at RT because of their low conductivity (see section 2.1.6). All the solid-state polymer-based cells listed in Table 4 were tested at least at 55 °C, while other SSNBs frequently can be operated at RT. High operation temperature of solid-state polymers generally prevent the commercialization of their SSNBs. Higher conductivity is significant for solid-state polymers, because it is almost the only bottleneck towards practical applications.

3. Summary

In summary, by categorizing the SSEs into NaSICONs, β/β"-aluminas, other oxides, sulfides, boranes and polymers, and benchmarking the key parameters of ionic conductivity, chemical stabilities, mechanical properties, interface compatibilities with sodium metal as well as the galvanostatic cycling and full-cell performance of SSNBs to state-of-the-art 18650 commercial Li-ion batteries, we reviewed recent advances in SSEs for SSNBs and evaluated their practical applicability. The following conclusions and outlooks are drawn:

1. In general, the conductivity of SSEs is not a serious challenge for battery application. In almost all categories – of NaSICONs, β/β"-aluminas, other oxides, sulfides and boranes – several or few compositions can be found with sufficiently high conductivity. Only solid-state polymers show insufficient conductivity at RT. The search for compositions with higher conductivity is therefore still important for this type of SSEs. Sb-based sulfides and carba-borohydrides show the highest potential of all SSEs.
2. Oxides show the highest chemical and thermal stabilities of all SSEs. Abundant data are available for the electrochemical windows of the SSEs. However, the evaluation of SSE electrochemical stability with respect to practical applications by means of calculated electrochemical windows is not precise, because interphases and kinetic inhibition have not been taken into consideration. When no water vapor is present in the environment, oxides, sulfides and boranes are all generally applicable in ambient drying room conditions, whereby oxides have the highest chemical and thermal stability. It is still too early to evaluate the mechanical stability of SSEs. However, stationary applications lower the demands on mechanical stability and with respect to large storage units, these will be packed in materials with higher fracture toughness than the SSEs.
3. Although not as good as state-of-the-art 18650 Li-ion batteries, Na/SSE/Na symmetric cells show closely comparable performances. In comparison, SSNB full cells are still far from practical applications. The cathode/electrolyte interfaces are regarded as the main reason, which may be solved, on the one hand, by means of infiltrating cathode materials into electrolyte backbones for oxides, or, on the other hand, by material or structural optimization for sulfides or boranes.

4. Outlook

As mentioned in section 2.4, in almost all existing reports on SSNBs the areal capacity (mAh cm^{-2}) is used instead of the industrially preferred gravimetric energy density (Wh kg^{-1}) to evaluate the cells, indicating the barrier between the current academic developments and industrial requirement. Academically the efforts are still mainly focused on various interfaces, while industry needs more effective materials per unit weight or volume together with stable performance in large scale applications. To bridge the gap, the key point is a scale-up of battery cell dimensions without changing the performances under laboratory conditions. Table 3 and Table 4 indicate that the development of SSNBs is approaching the targeted academic milestone of 3 mAh cm^{-2}. With larger battery components the attention will gradually shift from scientific feasibility to engineering development. Strategically, anode-less designs should be further explored to increase the energy density. Here the Na metal anode is formed during the charge process from cathode side. The electrolyte layer should be as thin as possible applying established processing methods. When dendrite formation can be fully prevented, μm-level or even thinner electrolyte layers will further increase the energy density of the full cell. The most difficult part is the cathode, because currently no cathode materials with high ionic conductivity is available. For compensating the sluggish ionic conductivity in the cathode material, so far electrolyte material has to be added to the cathode layer, which decreases the energy density. An electrolyte backbone together with infiltrated cathode active material is actually regarded as the most promising design for SSNB cathodes. In future, the electrolyte backbone should have high porosity of over 70% to decrease the amount of electrolyte material in cathodes and pores should be fully filled up by cathode active material to increase the energy density. Further scale-up of SSNB production depends on industrially preferred processes like tape casting or roll-to-roll deposition techniques. Because of the rigid nature of the SSNBs compared to LBE-based batteries, the stacking of large single cells (>100 cm^2 per cell) should have a realistic design for practical applications. Surely, the realization strongly relies on engineering skills. Solid-state polymers are special because they almost have only one bottleneck towards practical applications, the conductivity. When a solid-state polymer with the conductivity of 10^{-3} S cm^{-1} at RT is found, it has great potential to be commercialized

based on the existing industrialized technologies for polymer-based batteries.

Scientifically, the main task is still to find materials with better properties and performances. Ultimately, finding new materials with better properties compared to existing materials could always be the breakthrough for the whole research field. The possible strategy to find better SSEs was extensively discussed with respect to computational simulations.[79,193] When electrolyte materials will be discovered with even higher conductivity and stability compared to the materials mentioned in this review, and at the same time a cathode material with high electronic and high ionic conductivity as well as high specific capacity is also found, the resulting cells will be the breakthrough.

Acknowledgements

Part of this work was compiled in the project "BenchBatt" (reference no. 03XP0047B) and the authors acknowledge funding from the German Federal Ministry of Education and Research (BMBF). The authors take responsibility for the content of this publication.

Conflict of Interest

The authors declare no conflict of interest.

Keywords: energy-storage device · solid-state sodium battery · solid-state electrolyte · key parameters for battery · interfaces

[1] Z. Yang, J. Zhang, M. C. Kintner-Meyer, X. Lu, D. Choi, J. P. Lemmon, J. Liu, *Chem. Rev.* **2011**, *111*, 3577–3613.
[2] B. Dunn, H. Kamath, J.-M. Tarascon, *Science* **2011**, *334*, 928–935.
[3] D. Larcher, J.-M. Tarascon, *Nat. Chem.* **2015**, *7*, 19.
[4] H. Pan, Y.-S. Hu, L. Chen, *Energy Environ. Sci.* **2013**, *6*, 2338–2360.
[5] M. D. Slater, D. Kim, E. Lee, C. S. Johnson, *Adv. Funct. Mater.* **2013**, *23*, 947–958.
[6] N. Yabuuchi, K. Kubota, M. Dahbi, S. Komaba, *Chem. Rev.* **2014**, *114*, 11636–11682.
[7] C. Jiang, H. Li, C. Wang, *Sci. Bull.* **2017**, *62*, 1473–1490.
[8] L. Fan, S. Wei, S. Li, Q. Li, Y. Lu, *Adv. Energy Mater.* **2018**, *8*, 1702657.
[9] A. Aboulaich, R. Bouchet, G. Delaizir, V. Seznec, L. Tortet, M. Morcrette, P. Rozier, J. M. Tarascon, V. Viallet, M. Dollé, *Adv. Energy Mater.* **2011**, *1*, 179–183.
[10] A. Hayashi, K. Noi, A. Sakuda, M. Tatsumisago, *Nat. Commun.* **2012**, *3*, 856.
[11] K. Takada, *Acta Mater.* **2013**, *61*, 759–770.
[12] A. L. Robinson, J. Janek, *MRS Bull.* **2014**, *39*, 1046–1047.
[13] Y. Kato, S. Hori, T. Saito, K. Suzuki, M. Hirayama, A. Mitsui, M. Yonemura, H. Iba, R. Kanno, *Nat. Energyy* **2016**, *1*, 16030.
[14] J. Janek, W. G. Zeier, *Nat. Energy* **2016**, *1*, 16141.
[15] P. Albertus, S. Babinec, S. Litzelman, A. Newman, *Nat. Energy* **2018**, *3*, 16.
[16] C. Zhao, L. Liu, X. Qi, Y. Lu, F. Wu, J. Zhao, Y. Yu, Y. S. Hu, L. Chen, *Adv. Energy Mater.* **2018**, *8*, 1703012.
[17] W. Hou, X. Guo, X. Shen, K. Amine, H. Yu, J. Lu, *Nano Energy* **2018**, *52*, 279–291.
[18] Y. Lu, L. Li, Q. Zhang, Z. Niu, J. Chen, *Joule* **2018**, *2*, 1747–1770.
[19] D. Ruiz-Martínez, A. Kovacs, R. Gómez, *Energy Environ. Sci.* **2017**, *10*, 1936–1941.
[20] J. J. Kim, K. Yoon, I. Park, K. Kang, *Small Methods* **2017**, *1*, 1700219.
[21] Z. Jian, L. Zhao, H. Pan, Y.-S. Hu, H. Li, W. Chen, L. Chen, *Electrochem. Commun.* **2012**, *14*, 86–89.
[22] W. Guan, B. Pan, P. Zhou, J. Mi, D. Zhang, J. Xu, Y. Jiang, *ACS Appl. Mater. Interfaces* **2017**, *9*, 22369–22377.
[23] W. Pan, W. Guan, S. Liu, B. B. Xu, C. Liang, H. Pan, M. Yan, Y. Jiang, *J. Mater. Chem. A* **2019**, *7*, 13197–13204.
[24] Z. Yu, J. Song, M. L. Gordin, R. Yi, D. Tang, D. Wang, *Adv. Sci.* **2015**, *2*, 1400020.
[25] B. L. Ellis, L. F. Nazar, *Curr. Opin. Solid State Mater. Sci.* **2012**, *16*, 168–177.
[26] K. B. Hueso, M. Armand, T. Rojo, *Energy Environ. Sci.* **2013**, *6*, 734–749.
[27] J. T. Kummer, N. Weber, *SAE Trans.* **1968**, 1003–1028.
[28] J. T. Kummer, W. Neill, In *Battery having a molten alkali metal anode and a molten sulfur cathode*, US patent 3413150, **1968**.
[29] R. Bones, J. Coetzer, R. Galloway, D. Teagle, *J. Electrochem. Soc.* **1987**, *134*, 2379–2382.
[30] X. Lu, G. Xia, J. P. Lemmon, Z. Yang, *J. Power Sources* **2010**, *195*, 2431–2442.
[31] L. Xu, J. Li, C. Liu, G. Zou, H. Hou, X. Ji, *Acta Phys.-Chim. Sin.* **2020**, *36*, 1905013.
[32] J. W. Fergus, *Solid State Ionics* **2012**, *227*, 102–112.
[33] A. F. De Anastro, N. Lago, C. Berlanga, M. Galcerán, M. Hilder, M. Forsyth, D. Mecerreyes, *J. Membr. Sci.* **2019**, *582*, 435–441.
[34] M. Forsyth, L. Porcarelli, X. Wang, N. Goujon, D. Mecerreyes, *Acc. Chem. Res.* **2019**, *52*, 686–694.
[35] J. Yang, H. Zhang, Q. Zhou, H. Qu, T. Dong, M. Zhang, B. Tang, J. Zhang, G. Cui, *ACS Appl. Mater. Interfaces* **2019**, *11*, 17109–17127.
[36] J. B. Quinn, T. Waldmann, K. Richter, M. Kasper, M. Wohlfahrt-Mehrens, *J. Electrochem. Soc.* **2018**, *165*, A3284-A3291.
[37] https://lygte-info.dk/info/batteryIndex.html. 2019.
[38] P. Stallworth, J. Fontanella, M. Wintersgill, C. D. Scheidler, J. J. Immel, S. Greenbaum, A. Gozdz, *J. Power Sources* **1999**, *81*, 739–747.
[39] A. Ponrouch, E. Marchante, M. Courty, J.-M. Tarascon, M. R. Palacín, *Energy Environ. Sci.* **2012**, *5*, 8572–8583.
[40] J. Schnell, F. Tietz, C. Singer, A. Hofer, N. Billot, G. Reinhart, *Energy Environ. Sci.* **2019**, *12*, 1818–1833.
[41] R. MacMullin, G. Muccini, *AIChE J.* **1956**, *2*, 393–403.
[42] Z. Zhang, Y. Shao, B. Lotsch, Y.-S. Hu, H. Li, J. Janek, L. F. Nazar, C.-W. Nan, J. Maier, M. Armand, *Energy Environ. Sci.* **2018**, *11*, 1945–1976.
[43] C.-L. Tsai, Q. Ma, C. Dellen, S. Lobe, F. Vondahlen, A. Windmüller, D. Grüner, H. Zheng, S. Uhlenbruck, M. Finsterbusch, *Sustain. Energ. Fuels* **2019**, *3*, 280–291.
[44] W. Archer, R. Armstrong, D. Sellick, W. Bugden, J. Duncan, *J. Mater. Sci.* **1980**, *15*, 2066–2072.
[45] G. May, A. Hooper, *J. Mater. Sci.* **1978**, *13*, 1480–1486.
[46] http://www.ionotec.com/conductive-ceramics.html. 2019.
[47] R. C. Galloway, *J. Electrochem. Soc.* **1987**, *134*, 256.
[48] Q. Ma, M. Guin, S. Naqash, C.-L. Tsai, F. Tietz, O. Guillon, *Chem. Mater.* **2016**, *28*, 4821–4828.
[49] H.-P. Hong, *Mater. Res. Bull.* **1976**, *11*, 173–182.
[50] J. B. Goodenough, H.-P. Hong, J. Kafalas, *Mater. Res. Bull.* **1976**, *11*, 203–220.
[51] M. Guin, F. Tietz, *J. Power Sources* **2015**, *273*, 1056–1064.
[52] U. Von Alpen, M. Bell, W. Wichelhaus, *Mater. Res. Bull.* **1979**, *14*, 1317–1322.
[53] A. Hooper, *Chem. Interf. Electrochem.* **1980**, *109*, 161–166.
[54] D. T. Qui, J. Capponi, J. Joubert, R. Shannon, *J. Solid State Chem.* **1981**, *39*, 219–229.
[55] R. J. Cava, E. M. Vogel, D. W. Johnson Jr, *J. Am. Ceram. Soc.* **1982**, *65*, c157-c159.
[56] H. Perthuis, P. Colomban, *Mater. Res. Bull.* **1984**, *19*, 621–631.
[57] N. Gasmi, N. Gharbi, H. Zarrouk, P. Barboux, R. Morineau, J. Livage, *J. Sol-Gel Sci. Technol.* **1995**, *4*, 231–237.
[58] N. Bukun, *Ionics* **1996**, *2*, 63–68.
[59] H.-B. Kang, N.-H. Cho, *J. Mater. Sci.* **1999**, *34*, 5005–5013.
[60] J. Dygas, G. Fafilek, M. Breiter, *Solid State Ionics* **1999**, *119*, 115–125.
[61] E. Traversa, L. Montanaro, H. Aono, Y. Sadaoka, *J. Electroceram.* **2000**, *5*, 261–272.
[62] Z. Khakpour, *Electrochim. Acta.* **2016**, *196*, 337–347.
[63] H. Park, K. Jung, M. Nezafati, C.-S. Kim, B. Kang, *ACS Appl. Mater. Interfaces* **2016**, *8*, 27814–27824.
[64] S. Naqash, Q. Ma, F. Tietz, O. Guillon, *Solid State Ionics* **2017**, *302*, 83–91.
[65] Z. Zhang, Z. Zou, K. Kaup, R. Xiao, S. Shi, M. Avdeev, Y. S. Hu, D. Wang, B. He, H. Li, *Adv. Energy Mater.* **2019**, 1902373.

[66] S. Yde-Andersen, J. S. Lundsgaard, L. Møller, J. Engell, *Solid State Ionics* **1984**, *14*, 73–79.
[67] Q. Ma, C.-L. Tsai, X.-K. Wei, M. Heggen, F. Tietz, J. T. Irvine, *J. Mater. Chem. A* **2019**, *7*, 7766–7776.
[68] S. Naqash, D. Sebold, F. Tietz, O. Guillon, *J. Am. Ceram. Soc.* **2019**, *102*, 1057–1070.
[69] K. A. Wallroth, *Bull. Soc. Chim.* **1883**, *39*, 316.
[70] B. Matković, M. Šljukić, *Croat. Chem. Acta.* **1965**, *37*, 115–116.
[71] M. E. Brownfield, E. E. Foord, S. J. Sutley, T. Botinelly, *Am. Mineral.* **1993**, *78*, 653–656.
[72] Z. Zhang, Q. Zhang, J. Shi, Y. S. Chu, X. Yu, K. Xu, M. Ge, H. Yan, W. Li, L. Gu, *Adv. Energy Mater.* **2017**, *7*, 1601196.
[73] R. O. Fuentes, F. M. Figueiredo, M. R. Soares, F. M. B. Marques, *J. Eur. Ceram. Soc.* **2005**, *25*, 455–462.
[74] E. Vogel, R. J. Cava, E. Rietman, *Solid State Ionics* **1984**, *14*, 1–6.
[75] M. Guin, F. Tietz, O. Guillon, *Solid State Ionics* **2016**, *293*, 18–26.
[76] M. Samiee, B. Radhakrishnan, Z. Rice, Z. Deng, Y. S. Meng, S. P. Ong, J. Luo, *J. Power Sources* **2017**, *347*, 229–237.
[77] S. Song, H. M. Duong, A. M. Korsunsky, N. Hu, L. Lu, *Sci. Rep.* **2016**, *6*, 32330.
[78] P. P. Kumar, S. Yashonath, *J. Phy. Chem. B* **2002**, *106*, 7081–7089.
[79] H. Che, S. Chen, Y. Xie, H. Wang, K. Amine, X.-Z. Liao, Z.-F. Ma, *Energy Environ. Sci.* **2017**, *10*, 1075–1101.
[80] G. Rankin, H. Merwin, *J. Am. Chem. Soc.* **1916**, *38*, 568–588.
[81] R. R. Ridgway, A. A. Klein, W. J. O'Leary, *Trans. Electrochem. Soc.* **1936**, *70*, 71–88.
[82] J. Thèry, D. Briançon, *C. R. Hebd. Séances Acad. Sci.* **1962**, *254*, 2782.
[83] G. Yamaguchi, K. Suzuki, *Bull. Chem. Soc. Jpn.* **1968**, *41*, 93–99.
[84] J. Kummer, *Prog. Solid State Chem.* **1972**, *7*, 141–175.
[85] M. Bettman, C. R. Peters, *J. Phys. Chem.* **1969**, *73*, 1774–1780.
[86] M. S. Whittingham, R. A. Huggins, *J. Chem. Phys.* **1971**, *54*, 414–416.
[87] J. Briant, G. Farrington, *J. Solid State Chem.* **1980**, *33*, 385–390.
[88] A. Hooper, *J. Phys. D* **1977**, *10*, 1487.
[89] Y. Sheng, P. Sarkar, P. S. Nicholson, *J. Mater. Sci.* **1988**, *23*, 958–967.
[90] X. Lu, M. E. Bowden, V. L. Sprenkle, J. Liu, *Adv. Mater.* **2015**, *27*, 5915–5922.
[91] T. Wu, Z. Wen, C. Sun, X. Wu, S. Zhang, J. Yang, *J. Mater. Chem. A* **2018**, *6*, 12623–12629.
[92] E. Yi, E. Temeche, R. M. Laine, *J. Mater. Chem. A* **2018**.
[93] M. C. Bay, M. Wang, R. Grissa, M. V. Heinz, J. Sakamoto, C. Battaglia, *Adv. Energy Mater.* **2019**, 1902899.
[94] H.-P. Hong, J. Kafalas, M. Bayard, *Mater. Res. Bull.* **1978**, *13*, 757–761.
[95] R. Shannon, B. Taylor, T. Gier, H. Chen, T. Berzins, *Inorg. Chem.* **1978**, *17*, 958–964.
[96] J. J. Bentzen, P. S. Nicholson, *Mater. Res. Bull.* **1982**, *17*, 541–548.
[97] Y. Sadaoka, M. Matsuguchi, Y. Sakai, K. Komatsubara, *J. Mater. Sci.* **1992**, *27*, 5045–5051.
[98] J. J. Bentzen, P. S. Nicholson, *Mater. Res. Bull.* **1980**, *15*, 1737–1745.
[99] K. Yamashita, T. Nojiri, T. Umegaki, T. Kanazawa, *Solid State Ionics* **1989**, *35*, 299–306.
[100] T. Okura, H. Monma, K. Yamashita, *Solid State Ionics* **2004**, *172*, 561–564.
[101] K. Yamashita, T. Umegaki, M. Tanaka, T. Kakuta, T. Nojiri, *J. Electrochem. Soc.* **1996**, *143*, 2180–2186.
[102] M. A. Evstigneeva, V. B. Nalbandyan, A. A. Petrenko, B. S. Medvedev, A. A. Kataev, *Chem. Mater.* **2011**, *23*, 1174–1181.
[103] V. Nalbandyan, A. Petrenko, M. Evstigneeva, *Solid State Ionics* **2013**, *233*, 7–11.
[104] O. Smirnova, R. Fuentes, F. Figueiredo, V. Kharton, F. Marques, *J. Electroceram.* **2003**, *11*, 179–189.
[105] M. Neyret, M. Lenoir, A. Grandjean, N. Massoni, B. Penelon, M. Malki, *J. Non-Cryst. Solids.* **2015**, *410*, 74–81.
[106] Y. K. Startsev, A. Pronkin, I. Sokolov, I. Murin, *Glass Phys. Chem.* **2011**, *37*, 263–282.
[107] B. Maksimov, B. Litvin, V. Ilyukhin, N. Belov, *Sov. Phys. Crystallogr.* **1969**, *14*, 410.
[108] H. Beyeler, R. Shannon, H. Chen, *Appl. Phys. Lett.* **1980**, *37*, 934–935.
[109] P. Knauth, *Solid State Ionics* **2009**, *180*, 911–916.
[110] M. Jansen, U. Henseler, *J. Solid State Chem.* **1992**, *99*, 110–119.
[111] A. Hayashi, K. Noi, N. Tanibata, M. Nagao, M. Tatsumisago, *J. Power Sources* **2014**, *258*, 420–423.
[112] H. Wang, Y. Chen, Z. D. Hood, G. Sahu, A. S. Pandian, J. K. Keum, K. An, C. Liang, *Angew. Chem. Int. Ed.* **2016**, *55*, 8551–8555; *Angew. Chem.* **2016**, *128*, 8693–8697.
[113] T. W. Kim, K. H. Park, Y. E. Choi, J. Y. Lee, Y. S. Jung, *J. Mater. Chem. A* **2018**, *6*, 840–844.
[114] J. W. Heo, A. Banerjee, K. H. Park, Y. S. Jung, S. T. Hong, *Adv. Energy Mater.* **2018**, *8*, 1702716.
[115] A. Hayashi, N. Masuzawa, S. Yubuchi, F. Tsuji, C. Hotehama, A. Sakuda, M. Tatsumisago, *Nat. Commun.* **2019**, *10*, 1–6.
[116] M. Duchardt, U. Ruschewitz, S. Adams, S. Dehnen, B. Roling, *Angew. Chem. Int. Ed.* **2018**, *57*, 1351–1355; *Angew. Chem.* **2018**, *130*, 1365–1369.
[117] Z. Zhang, E. Ramos, F. Lalère, A. Assoud, K. Kaup, P. Hartman, L. F. Nazar, *Energy Environ. Sci.* **2018**, *11*, 87–93.
[118] L. Zhang, K. Yang, J. Mi, L. Lu, L. Zhao, L. Wang, Y. Li, H. Zeng, *Adv. Energy Mater.* **2015**, *5*, 1501294.
[119] N. Wang, K. Yang, L. Zhang, X. Yan, L. Wang, B. Xu, *J. Mater. Sci.* **2018**, *53*, 1987–1994.
[120] M. Ribes, B. Barrau, J. Souquet, *J. Non-Cryst. Solids* **1980**, *38*, 271–276.
[121] S. Susman, L. Boehm, K. Volin, C. Delbecq, *Solid State Ionics* **1981**, *5*, 667–669.
[122] W. Yao, S. W. Martin, *Solid State Ionics* **2008**, *178*, 1777–1784.
[123] K. Noi, A. Hayashi, M. Tatsumisago, *J. Power Sources* **2014**, *269*, 260–265.
[124] N. Kamaya, K. Homma, Y. Yamakawa, M. Hirayama, R. Kanno, M. Yonemura, T. Kamiyama, Y. Kato, S. Hama, K. Kawamoto, *Nat. Mater.* **2011**, *10*, 682.
[125] J. Irvine, A. West, *Solid State Ionics* **1988**, *28*, 214–219.
[126] A. Banerjee, K. H. Park, J. W. Heo, Y. J. Nam, C. K. Moon, S. M. Oh, S. T. Hong, Y. S. Jung, *Angew. Chem. Int. Ed.* **2016**, *55*, 9634–9638; *Angew. Chem.* **2016**, *128*, 9786–9790.
[127] M. Matsuo, S. Kuromoto, T. Sato, H. Oguchi, H. Takamura, S.-i. Orimo, *Appl. Phys. Lett.* **2012**, *100*, 203904.
[128] W. S. Tang, M. Matsuo, H. Wu, V. Stavila, W. Zhou, A. A. Talin, A. V. Soloninin, R. V. Skoryunov, O. A. Babanova, A. V. Skripov, *Adv. Energy Mater.* **2016**, *6*, 1502237.
[129] W. S. Tang, K. Yoshida, A. V. Soloninin, R. V. Skoryunov, O. A. Babanova, A. V. Skripov, M. Dimitrievska, V. Stavila, S.-i. Orimo, T. J. Udovic, *ACS Energy Lett.* **2016**, *1*, 659–664.
[130] T. J. Udovic, M. Matsuo, W. S. Tang, H. Wu, V. Stavila, A. V. Soloninin, R. V. Skoryunov, O. A. Babanova, A. V. Skripov, J. J. Rush, *Adv. Mater.* **2014**, *26*, 7622–7626.
[131] T. J. Udovic, M. Matsuo, A. Unemoto, N. Verdal, V. Stavila, A. V. Skripov, J. J. Rush, H. Takamura, S.-i. Orimo, *Chem. Commun.* **2014**, *50*, 3750–3752.
[132] W. S. Tang, A. Unemoto, W. Zhou, V. Stavila, M. Matsuo, H. Wu, S.-i. Orimo, T. J. Udovic, *Energy Environ. Sci.* **2015**, *8*, 3637–3645.
[133] L. Duchene, R. S. Kuhnel, D. Rentsch, A. Remhof, H. Hagemann, C. Battaglia, *Chem. Commun.* **2017**, *53*, 4195–4198.
[134] D. E. Fenton, J. M. Parker, P. V. Wright, *Polymer* **1973**, *14*, 589.
[135] J. Mindemark, M. J. Lacey, T. Bowden, D. Brandell, *Prog. Polym. Sci.* **2018**, *81*, 114–143.
[136] W. Niu, L. Chen, Y. Liu, L.-Z. Fan, *Chem. Eng. J.* **2020**, *384*, 123233.
[137] Q. Zhang, Y. Lu, H. Yu, G. Yang, Q. Liu, Z. Wang, L. Chen, Y.-S. Hu, *J. Electrochem. Soc.* **2020**, *167*, 070523.
[138] J.-F. Wu, Z.-Y. Yu, Q. Wang, X. Guo, *Energy Storage Mater.* **2020**, *24*, 467–471.
[139] C. Zhao, L. Liu, Y. Lu, M. Wagemaker, L. Chen, Y. S. Hu, *Angew. Chem. Int. Ed.* **2019**, *58*, 17026–17032.
[140] X. Yu, L. Xue, J. B. Goodenough, A. Manthiram, *ACS Mater. Lett.* **2019**, *1*, 132–138.
[141] X. Wang, X. Zhang, Y. Lu, Z. Yan, Z. Tao, D. Jia, J. Chen, *ChemElectroChem.* **2018**, *5*, 3628–3632.
[142] C. Ma, K. Dai, H. Hou, X. Ji, L. Chen, D. G. Ivey, W. Wei, *Adv. Sci.* **2018**, *5*, 1700996.
[143] K. Freitag, P. Walke, T. Nilges, H. Kirchhain, R. Spranger, L. van Wüllen, *J. Power Sources* **2018**, *378*, 610–617.
[144] Z. Zhang, K. Xu, X. Rong, Y.-S. Hu, H. Li, X. Huang, L. Chen, *J. Power Sources* **2017**, *372*, 270–275.
[145] Y. Yao, Z. Wei, H. Wang, H. Huang, Y. Jiang, X. Wu, X. Yao, Z. S. Wu, Y. Yu, *Adv. Energy Mater.* **2020**, *10*, 1903698.
[146] C. Sångeland, R. Younesi, J. Mindemark, D. Brandell, *Energy Storage Mater.* **2019**, *19*, 31–38.
[147] M. Vahini, M. Muthuvinayagam, *J. Mater. Sci. Mater. Electron.* **2019**, *30*, 5609–5619.
[148] X. Zhang, X. Wang, S. Liu, Z. Tao, J. Chen, *Nano Res.* **2018**, *11*, 6244–6251.

[149] S. Chen, F. Feng, Y. Yin, H. Che, X.-Z. Liao, Z.-F. Ma, *J. Power Sources* **2018**, *399*, 363–371.
[150] Y. Zheng, Q. Pan, M. Clites, B. W. Byles, E. Pomerantseva, C. Y. Li, *Adv. Energy Mater.* **2018**, *8*, 1801885.
[151] D. F. Shriver, R. Dupon, M. Stainer, *J. Power Sources* **1983**, *9*, 383–388.
[152] A. Basile, M. Hilder, F. Makhlooghiazad, C. Pozo-Gonzalo, D. R. MacFarlane, P. C. Howlett, M. Forsyth, *Adv. Energy Mater.* **2018**, *8*, 1703491.
[153] M. Forsyth, T. Chimdi, A. Seeber, D. Gunzelmann, P. C. Howlett, *J. Mater. Chem. A* **2014**, *2*, 3993–4003.
[154] S. Chen, F. Feng, Y. Yin, X. Lizo, Z. Ma, *Energy Storage Mater.* **2019**, *22*, 57–65.
[155] F. Makhlooghiazad, D. Gunzelmann, M. Hilder, D. R. MacFarlane, M. Armand, P. C. Howlett, M. Forsyth, *Adv. Energy Mater.* **2017**, *7*, 1601272.
[156] A. Bhide, J. Hofmann, A. K. Dürr, J. Janek, P. Adelhelm, *Phys. Chem. Chem. Phys.* **2014**, *16*, 1987–1998.
[157] C. Bernuy-Lopez, W. Manalastas Jr, J. M. Lopez del Amo, A. Aguadero, F. Aguesse, J. A. Kilner, *Chem. Mater.* **2014**, *26*, 3610–3617.
[158] V. Lacivita, Y. Wang, S.-H. Bo, G. Ceder, *J. Mater. Chem. A* **2019**, *7*, 8144–8155.
[159] A. Bitner-Michalska, G. M. Nolis, G. Żukowska, A. Zalewska, M. Poterała, T. Trzeciak, M. Dranka, M. Kalita, P. Jankowski, L. Niedzicki, *Sci. Rep.* **2017**, *7*, 1–10.
[160] R. Chen, Q. Li, X. Yu, L. Chen, H. Li, *Chem. Rev.* **2019**.
[161] R. Fuentes, F. Figueiredo, F. Marques, J. Franco, *Solid State Ionics* **2001**, *139*, 309–314.
[162] E. Dashjav, Q. Ma, Q. Xu, C.-L. Tsai, M. Giarola, G. Mariotto, F. Tietz, *Solid State Ionics* **2018**, *321*, 83–90.
[163] M. Guin, S. Indris, M. Kaus, H. Ehrenberg, F. Tietz, O. Guillon, *Solid State Ionics* **2017**, *302*, 102–106.
[164] G. Flor, A. Marini, V. Massarotti, M. Villa, *Solid State Ionics* **1981**, *2*, 195–204.
[165] J. B. Bates, D. Dohy, R. Anderson, *J. Mater. Sci.* **1985**, *20*, 3219–3229.
[166] G. McConohy, A. C. Baclig, A. D. Poletayev, J. Park, W. C. Chueh, *Solid State Ionics* **2019**, *337*, 82–90.
[167] S.-L. Shang, Z. Yu, Y. Wang, D. Wang, Z.-K. Liu, *ACS Appl. Mater. Interfaces* **2017**, *9*, 16261–16269.
[168] Y. Tian, Y. Sun, D. C. Hannah, Y. Xiao, H. Liu, K. W. Chapman, S.-H. Bo, G. Ceder, *Joule* **2019**, *3*, 1037–1050.
[169] E. Muetterties, J. Balthis, Y. Chia, W. Knoth, H. Miller, *Inorg. Chem.* **1964**, *3*, 444–451.
[170] S. Körbe, P. J. Schreiber, J. Michl, *Chem. Rev.* **2006**, *106*, 5208–5249.
[171] K. Liu, Y. Liu, D. Lin, A. Pei, Y. Cui, *Sci. Adv.* **2018**, *4*, eaas9820.
[172] X. Feng, M. Ouyang, X. Liu, L. Lu, Y. Xia, X. He, *Energ. Storage Mater.* **2018**, *10*, 246–267.
[173] Y. Wang, W. H. Zhong, *ChemElectroChem.* **2015**, *2*, 22–36.
[174] J. Zhu, X. Zhang, E. Sahraei, T. Wierzbicki, *J. Power Sources* **2016**, *336*, 332–340.
[175] E. Sahraei, M. Kahn, J. Meier, T. Wierzbicki, *RSC Adv.* **2015**, *5*, 80369–80380.
[176] J. F. Nonemacher, S. Naqash, F. Tietz, J. Malzbender, *Ceram. Int.* **2019**, *45*, 21308–21314.
[177] W. Zhou, Y. Li, S. Xin, J. B. Goodenough, *ACS Cent. Sci.* **2017**, *3*, 52–57.
[178] Y. Lu, J. A. Alonso, Q. Yi, L. Lu, Z. L. Wang, C. Sun, *Adv. Energy Mater.* **2019**, 1901205.
[179] E. Matios, H. Wang, C. Wang, X. Hu, X. Lu, J. Luo, W. Li, *ACS Appl. Mater. Interfaces* **2019**, *11*, 5064–5072.
[180] H. Wan, J. P. Mwizerwa, X. Qi, X. Xu, H. Li, Q. Zhang, L. Cai, Y. S. Hu, X. Yao, *ACS Appl. Mater. Interfaces* **2018**, *10*, 12300–12304.
[181] N. J. Taylor, S. Stangeland-Molo, C. G. Haslam, A. Sharafi, T. Thompson, M. Wang, R. Garcia-Mendez, J. Sakamoto, *J. Power Sources* **2018**, *396*, 314–318.
[182] B. Lee, E. Paek, D. Mitlin, S. W. Lee, *Chem. Rev.* **2019**, *119*, 5416–5460.
[183] C.-L. Tsai, V. Roddatis, C. V. Chandran, Q. Ma, S. Uhlenbruck, M. Bram, P. Heitjans, O. Guillon, *ACS Appl. Mater. Interfaces* **2016**, *8*, 10617–10626.
[184] A. Sharafi, E. Kazyak, A. L. Davis, S. Yu, T. Thompson, D. J. Siegel, N. P. Dasgupta, J. Sakamoto, *Chem. Mater.* **2017**, *29*, 7961–7968.
[185] A. Lodding, J. Mundy, A. Ott, *Physica* **1970**, *38*, 559–569.
[186] J. N. Mundy, *Phys. Rev. B* **1971**, *3*, 2431.
[187] T. Krauskopf, H. Hartmann, W. G. Zeier, J. r Janek, *ACS Appl. Mater. Interfaces* **2019**, *11*, 14463–14477.
[188] P. Kehne, C. Guhl, Q. Ma, F. Tietz, L. Alff, R. Hausbrand, P. Komissinskiy, *J. Power Sources* **2019**, *409*, 86–93.
[189] T. Lan, C.-L. Tsai, F. Tietz, X.-K. Wei, M. Heggen, R. E. Dunin-Borkowski, R. Wang, Y. Xiao, Q. Ma, O. Guillon, *Nano Energy* **2019**, *65*, 104040.
[190] P. Kehne, C. Guhl, L. Alff, R. Hausbrand, P. Komissinskiy, *Solid State Ionics* **2019**, *341*, 115041.
[191] H. Yamauchi, J. Ikejiri, F. Sato, H. Oshita, T. Honma, T. Komatsu, *J. Am. Ceram. Soc.* **2019**, *102*, 6658–6667.
[192] L. Duchêne, R.-S. Kühnel, E. Stilp, E. C. Reyes, A. Remhof, H. Hagemann, C. Battaglia, *Energy Environ. Sci.* **2017**, *10*, 2609–2615.
[193] G. Åvall, J. Mindemark, D. Brandell, P. Johansson, *Adv. Energy Mater.* **2018**, *8*, 1703036.

Manuscript received: January 31, 2020
Revised manuscript received: May 27, 2020
Accepted manuscript online: May 28, 2020